HHS Public Access

Author manuscript

Cell Rep. Author manuscript; available in PMC 2021 October 25.

Published in final edited form as:

Cell Rep. 2021 June 15; 35(11): 109234. doi:10.1016/j.celrep.2021.109234.

Differential effect of sleep deprivation on place cell representations, sleep architecture, and memory in young and old mice

Robin K. Yuan[1,2,7], **Matthew R. Lopez**[3,7], **Manuel-Miguel Ramos-Alvarez**[4,7], **Marc E. Normandin**[3,7], **Arthur S. Thomas**[5], **David S. Uygun**[6], **Vanessa R. Cerda**[3], **Amandine E. Grenier**[3], **Matthew T. Wood**[3], **Celia M. Gagliardi**[3], **Herminio Guajardo**[3], **Isabel A. Muzzio**[3,8,*]

[1]Division of Sleep and Circadian Disorders, Departments of Medicine and Neurology, Brigham and Women's Hospital, 221 Longwood Avenue, Boston, MA, USA

[2]Division of Sleep Medicine, Harvard Medical School, 221 Longwood Avenue, Boston, MA, USA

[3]University of Texas at San Antonio, Department of Biology, One UTSA Circle, San Antonio, TX 78249, USA

[4]University of Jaen, Psychology Department, Campus Las Lagunillas, Jaen 23071, Spain

[5]Perelman School of Medicine, University of Pennsylvania, 3400 Civic Center Boulevard, Philadelphia, PA 19104, USA

[6]VA Boston Healthcare System and Department of Psychiatry, Harvard Medical School, West Roxbury, MA 02132, USA

[7]These authors contributed equally

[8]Lead contact

SUMMARY

Poor sleep quality is associated with age-related cognitive decline, and whether reversal of these alterations is possible is unknown. In this study, we report how sleep deprivation (SD) affects hippocampal representations, sleep patterns, and memory in young and old mice. After training in

*Correspondence: isabel.muzzio@utsa.edu.

AUTHOR CONTRIBUTIONS

R.K.Y. and M.R.L. conducted experiments, analyses, and wrote the manuscript; M.-M.R.-A. conducted statistical analyses and made figures; M.E.N. wrote code and conducted analysis; D.S.U. assisted with spindle analysis and provided code; A.S.T., V.R.C., A.E.G., M.T.W., C.M.G., and H.G. contributed to data collection and analysis; and I.A.M. supervised all experiments, analysis, and writing of the manuscript.

SUPPLEMENTAL INFORMATION

Supplemental information can be found online at https://doi.org/10.1016/j.celrep.2021.109234.

DECLARATION OF INTERESTS

The authors declare no competing interests. D.S.U. is Research Health Scientist at VA Boston Healthcare System, West Roxbury, MA. The content of this work does not represent the views of the US Department of Veterans Affairs of the United States Government.

INCLUSION AND DIVERSITY

One or more of the authors of this paper self-identifies as an underrepresented ethnic minority in science. One or more of the authors of this paper received support from a program designed to increase minority representation in science. While citing references scientifically relevant for this work, we also actively worked to promote gender balance in our reference list.

a hippocampus-dependent object-place recognition (OPR) task, control animals sleep *ad libitum*, although experimental animals undergo 5 h of SD, followed by recovery sleep. Young controls and old SD mice exhibit successful OPR memory, whereas young SD and old control mice are impaired. Successful performance is associated with two cellular phenotypes: (1) "context" cells, which remain stable throughout training and testing, and (2) "object configuration" cells, which remap when objects are introduced to the context and during testing. Additionally, effective memory correlates with spindle counts during non-rapid eye movement (NREM)/rapid eye movement (REM) sigma transitions. These results suggest SD may serve to ameliorate age-related memory deficits and allow hippocampal representations to adapt to changing environments.

Graphical Abstract

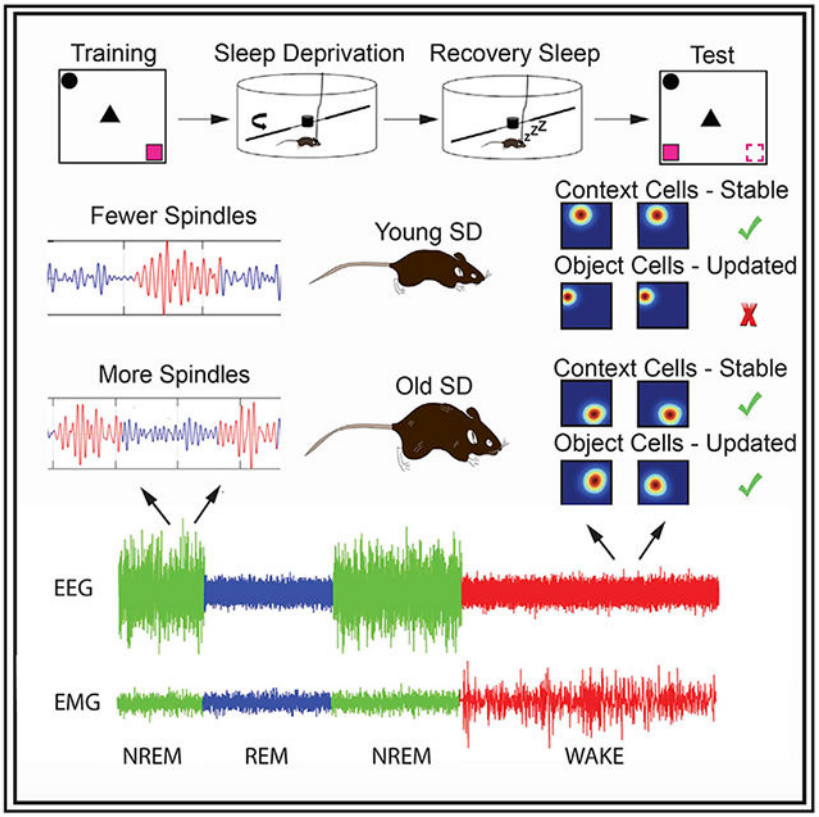

In brief

Age-related cognitive decline is associated with poor sleep quality. Yuan et al. show that acute sleep deprivation has beneficial effects on sleep microarchitecture, memory, and hippocampal representations in old mice and has opposite effects in young animals. These findings suggest that acute sleep deprivation may serve to mitigate age-related cognitive decline.

INTRODUCTION

A large amount of evidence suggests that sleep plays a key role in memory consolidation (Abel et al., 2013; Rasch and Born, 2013; Stickgold and Walker, 2013; Tononi and Cirelli,

2014). Studies have shown performance gains following post-training sleep (Gais and Born, 2004; Gais et al., 2006; Smith, 2001), as well as learning impairments when sleep deprivation (SD) is conducted after training (Graves et al., 2003; Prince et al.,2014; Smith and Rose, 1996). However, the effects of SD are complex and vary across the lifespan. For example, although SD produces deficits in psychomotor tasks in adolescents (de Bruin et al., 2017), its impact in adults is highly variable (Krause et al., 2017), with some studies showing within- and across-individual differences in cognitive susceptibility (Saletin et al., 2016; Wilson et al., 2019). Notably, although limiting sleep periods decreases insomnia in old subjects (Wennberg et al., 2013), it remains unclear whether this procedure also improves sleep quality and/or microarchitecture.

Sleep involves interspersed periods of non-rapid eye movement (NREM), a state characterized by high amplitude, low frequency (0.2–4 Hz), synchronous electroencephalographic (EEG) activity, and rapid eye movement (REM), a state characterized by low-amplitude fast desynchronized EEG waves. NREM is important for memory formation because it is thought that, during this stage, information is transferred to cortex for long-term storage (for a review, see Antony et al., 2019), whereas REM has been associated with both consolidation of novel information and forgetting of previously encoded information (Poe, 2017). During NREM, there are rapid bursts of activity (10–14 Hz) of short duration, known as spindles. Spindles are thought to facilitate memory reactivation, which is essential for proper consolidation (Rasch and Born, 2013). Critically, changes in NREM and spindle characteristics predict early memory impairments in old subjects (Taillard et al., 2019). However, it is unknown whether reversing these sleep alterations can have positive effects on cognition.

The hippocampus plays a critical role in the formation of episodic memories—recollections of events happening in specific contexts at particular times (Smith and Mizumori, 2006; Squire and Zola, 1998). It is assumed that the activity of hippocampal place cells, which fire in specific locations when animals navigate (O'Keefe and Dostrovsky, 1971), provides a cognitive map in which episodic events are embedded (Mizumori, 2006; Smith and Mizumori, 2006). In support of this idea, it has been shown that networks of hippocampal cells active during wake are reactivated during NREM sleep at compressed timescales (Drieu et al., 2018; Hwaun and Colgin, 2019; Lee and Wilson, 2002), which is important for memory formation (de Lavilléon et al., 2015).

Both sleep and cognition undergo age-related changes across the lifespan (Huang et al., 2002). Older humans exhibit more fragmented sleep, less slow-wave sleep, and alterations in spindle characteristics in comparison to young adults (Espiritu, 2008; Hasan et al., 2012; Ohayon et al., 2004; Clawson et al., 2016). Additionally, old subjects also show impairments in hippocampus-dependent cognitive tasks (Lester et al., 2017; Lister and Barnes, 2009; Miller and O'Callaghan, 2005). These observations have suggested that age-related cognitive decline may be related to the sleep changes (Altena et al., 2010). In this study, we investigated whether an acute period of SD could serve to modify subsequent sleep architecture, hippocampal place cell firing, and object and place recognition (OPR) memory in young and old mice. Our results indicate that SD has differential effects in young and old mice. In young mice, an acute SD session impairs memory, decreases the flexibility

of hippocampal representations, and reduces the number of spindles during NREM/REM sigma transitions. Conversely, in old animals, SD enhances memory and improves the quality of NREM microarchitecture and hippocampal representations. We suggest that acute SD allows the hippocampus to adapt to changing environments and reverses age-related memory deficits.

RESULTS

SD impairs OPR memory in young adult mice but enhances performance in old mice

Four groups of animals, including young controls (YCs) (n = 16), young SD (YSD) (n = 15), old control (OC) (n = 13), and old SD (OSD) (n = 15), were trained in the OPR task, as illustrated in Figure 1A. Analysis of object and place preference during the test showed an interaction between age and sleep condition ($Fw(1) = 0.55$; $p < 0.00001$). Simple effects revealed that the YCs and OSD displayed greater preference for the moved object in comparison to YSD and OC (YC × YSD: $Tw(16.07) = 3.39$, $p < 0.02$; YC × OC: $Tw(17.41) = 2.44$, $p < 0.03$; OC × OSD: $Tw(15.10) = 2.11$, $p < 0.05$; YSD × OSD: $Tw(15.89) = 2.99$, $p < 0.008$; Figure 1B). These results indicated that SD was beneficial in old animals, bringing their OPR performance to the level of young controls.

Experiments with rats have shown that animals display more exploration of familiar objects when the animals perceive the context as different (Cohen et al., 2013; Dix and Aggleton, 1999; Mumby et al., 2002). To determine whether failures in context recognition modulated preference for familiar object location, we calculated the percent change in preference for the unmoved objects. We found an interaction between age and sleep condition ($Fw(1) = 0.55$; $p < 0.0001$; Figure 1C). Single effects corroborated that YC and OSD mice displayed less preference for the unmoved objects (YC × YSD: $Tw(16.07) = 11.51$, $p < 0.01$; OC × OSD: $Tw(15.10) = 4.47$, $p < 0.05$), but there were no significant differences between the YSD and OCs (YSD × OC: $Tw(15.58) = 1.30$; $p = 0.26$), neither of which showed a preference for the unmoved objects. These data indicate that the poor OPR performance exhibited by YSD and OCs is not related to a shift in preference for objects placed in familiar locations.

We evaluated the total time exploring the objects across trials to confirm that there were no differences in locomotor activity. We found no significant effects of age, sleep condition, or interactions on total object exploration (age: $Fw(1) = 0.12$, $p = 0.73$; sleep: $Fw(1) = 0.07$, $p = 0.79$; interaction age × sleep: $Fw(1) = 0.31$, $p = 0.38$; interaction age × sleep × trial: $Fw(3) = 0.09$, $p = 0.81$). However, there was an effect of trial ($Fw(3) = 4.08$; $p < 0.0001$). Simple effects revealed that all groups displayed more total object exploration during the first object trial and the test (T1-T2: $Zw = 3.82$, $p < 0.0001$; T3-test: $Zw = 1.75$, $p < 0.04$; Figure 1D), which likely resulted from the initial novelty of the objects and the change in configuration, respectively. Because we observed this difference, we also calculated the percent change in object preference, excluding the first object trial to ensure that our results were not biased by the novelty of the objects. The results were almost identical to those including all trials (interaction age × sleep: Fw(1): 0.55, $p < 0.0001$; YC × YSD: $Tw(17.06) = 2.15$, $p < 0.05$; OD × OSD: $Tw(13.66) = 3.74$, $p < 0.003$; YC × OC: $Tw(16.13) = 2.34$,

$p < 0.04$; YSD × OSD: $Tw(14.50) = 3.66$, $p < 0.003$; Figure 1E), which indicated that the observed differences were not due to variability in object exploration.

The observation that old SD animals displayed better OPR performance suggested that post-learning SD followed by recovery sleep had a beneficial effect on memory. To determine whether this effect was time dependent, we delayed the SD by 5 h in a separate group of young (n = 6) and old (n = 7) animals. These mice were trained and tested exactly as described above but were allowed to sleep *ad libitum* for 5 h after training, prior to the SD procedure. This manipulation neither impaired young mice, which showed a preference for the moved object, nor rescued the memory impairments in old animals, which displayed no object preference during the test ($Tw(6.88) = 4.85$; $p < 0.002$; Figure 1F). These results indicate that there is a time window during which SD leads to memory deficits in young animals or ameliorates age-related cognitive decline in old ones.

Levels of corticosterone are similar in young and old sleep-restricted mice

Total or partial SD has been shown to induce mild stress in rodents (Coenen and van Luijtelaar, 1985; Tobler et al., 1983). Additionally, sleep alterations correlate with a rise in cortisol levels in older human subjects (Castello-Domenech et al., 2016; Morgan et al., 2017). We collected blood from young (n = 5) and old (n = 5) mice following 5 h of SD (experimental groups) or 5 h of *ad libitum* sleep (control groups) to determine whether our sleep manipulations had a differential effect on corticosterone levels. Although SD produced an increase in plasma corticosterone compared to normal sleep conditions ($F(1) = 16.85$; $p < 0.02$), there were no differences between the age groups ($F(1) = 0.29$; $p = 0.61$) or interactions between age and sleep condition ($F(1) = 0.04$; $p = 0.87$; Figure 1G). These data indicated that corticosterone levels could not account for the differences in performance between YSD and OSD mice.

Rate remapping increases during testing in YC and OSD animals

A subset of animals was implanted with tetrodes in area CA1 to determine the effects of SD on hippocampal neuronal activity during OPR memory (electrode positions are shown in Figures S1A). First, we corroborated that there were no differences in performance between tetrode or electroencephalogram (EEG)/electromyogram (EMG)-implanted animals (interaction between age and type of implant: $Fw(1) = 0.13$, $p = 0.72$; interaction between sleep condition and type of implant: $Fw(1) = 2.06$, $p = 0.17$). The groups displayed OPR memory patterns similar to those described in Figure 1B, which was evident in an interaction between age and sleep condition ($Fw(10) = 17.53$; $p < 0.001$). These results indicate that the type of implant did affect performance (Figure 2A).

Then, we examined place cell activity in 110 cells recorded in 10 young mice (60 cells in 6 controls and 50 cells in 4 SD mice) and 77 cells recorded in 10 old mice (36 cells in 5 controls and 41 cells in 5 SD mice). The quality of the isolated clusters was examined by calculating isolation distance, a parameter that evaluates the distance between the spikes of a particular cluster and other spikes or noise (Harris et al., 2001) and L-ratio, a parameter that estimates how well cluster spikes are separated from other spikes recorded from the same tetrode (Schmitzer-Torbert et al., 2005). There were no significant differences over time

and/or across groups (Figure 2B; isolation distance: interactions: age versus sleep condition: $Fw(1) = 0.14$, $p = 0.71$; age versus trial: $Fw(4) = 0.32$, $p = 0.87$; sleep condition versus trial: $Fw(4) = 0.20$, $p = 0.94$; age versus sleep condition versus trial: $Fw(4) = 0.11$, $p = 0.98$; Figure S1B: L-ratio: interactions: age versus sleep condition: $Fw(1) = 0.001$, $p = 0.97$; age versus trial: $Fw(4) = 0.31$, $p = 0.87$; sleep condition versus trial: $Fw(4) = 0.44$, $p = 0.78$; age versus sleep condition versus trial: $Fw(4) = 0.14$, $p = 0.97$). Then, we analyzed several place cell parameters. There were no significant effects of age, group, or interactions in mean, peak, or out-of-field firing rate, number of fields, field size, or spatial information content ($p > 0.05$; Figures S1C–S1H). These data indicate that place cell parameters did not differ between age groups or sleep conditions throughout training and testing.

Hippocampal cells have previously been shown to code environmental changes through increases or decreases in firing rate, a phenomenon known as rate remapping (Leutgeb et al., 2005). Therefore, we hypothesized that average firing activity could have masked potential rate-remapping differences. To assess this possibility, we calculated rate remapping as the absolute difference in peak firing rate for each cell across trials. This analysis revealed main effects of age ($Fw(1) = 10.20$; $p < 0.00001$) and trial ($Fw(3) = 2.12$; $p < 0.005$) and an interaction between age, trial, and sleep condition ($Fw(3) = 1.30$; $p < 0.05$). Analysis of simple effects indicated that rate remapping was different between the groups exclusively during the test trial. YCs and OSD animals, the two groups that exhibited successful learning, displayed more rate remapping than YSD during the test session (YC versus YSD: $Tw(46.29) = 2.30$, $p < 0.03$; YSD versus OSD: $Tw(29.79) = 3.93$, $p < 0.005$) and increased rate remapping during the test in comparison to the last training trial (T3 versus test: YC: $Zw = 1.69$, $p < 0.02$; OSD: $Zw = 2.80$, $p < 0.02$; Figure 2C). These results indicate that changes in rate remapping are important for updating OPR memory representations.

The overall stability of hippocampal representations decreases during the moved-object test in all groups

Hippocampal cells respond to spatial cues, including objects (Cohen et al., 2013). Therefore, we expected a shift in the cells' preferred firing location (i.e., global remapping) when the objects were first introduced (Hab versus T1) but short-term stability across the training trials when the objects and environment remained unchanged (T1–T3). We also anticipated global remapping during the test trial (test), reflecting the change in the object configuration. Analysis of similarity between place cell maps revealed significant effects of age ($Fw(1) = 8.32$; $p < 0.008$) and trial ($Fw(3) = 29.35$; $p < 0.000001$), as well as interactions of age and trial ($Fw(3) = 1.45$; $p < 0.04$) and sleep condition and trial ($Fw(3) = 1.63$; $p < 0.02$). Analysis of simple effects showed that old mice displayed more global remapping than young animals when the objects were first introduced ($Tw(98.60) = 2.95$; $p < 0.004$), which likely reflected the unstable nature of spatial representations in this group (Barnes et al., 1997). However, no differences in stability were observed during the object training trials (T1 versus T2: $Tw(101.10) = 1.08$, $p = 0.28$; T2 versus T3: $Tw(95.97) = 1.12$, $p = 0.26$). As expected, all groups displayed lower place field stability during the test trial in comparison to the high short-term stability observed during training ($p < 0.05$), with old animals displaying more instability than the young ones (T3 versus test: $Tw(91.84) = 3.40$;

$p < 0.001$; Figure 2D). These results indicate that all groups exhibit some global remapping during the moved-object test trial.

Distinct cell types are differentially affected by SD and age

We have previously observed that distinct CA1 subpopulations respond differently during fear learning (Wang et al., 2015). To determine whether the same happened during the OPR task, cells were classified according to their remapping patterns during training. The threshold used to classify place cell stability was determined using correlation scatterplots and distributions as well as a machine learning algorithm (Figures S2). Using these tools, we establish that a correlation of 0.35 was the best cutoff value to categorize the cells (e.g., cell correlations above 0.35 were considered stable and those below 0.35 unstable). "Context" cells displayed high stability throughout habituation and training; "object configuration" cells remapped when objects were first introduced but remained stable during all the object training sessions; and "unstable" cells remapped across all training sessions. As previously reported, we observed that object configuration cells were active in the context, even before the objects were introduced (Ásgeirsdóttir et al., 2020). Therefore, it is likely that these cells coded the arrangement of the objects in relation to contextual cues already present in the environment, rather than purely object-related firing. In young animals, each of these categories made up roughly 1/3 of the cells recorded. However, old animals had a lower percentage of stable context cells than young mice (Figures 2E and 2F).

After cells were classified, we examined similarity scores (e.g., the degree of global remapping) within each group across consecutive trials (Figure 3A). We hypothesized that, if animals remembered the environment, context cells should remain stable during the moved-object test but display instability if that was not the case. Context cells showed main effects of age ($Fw(1) = 7.87$; $p < 0.007$) and trial ($Fw(3) = 3.04$; $p < 0.0001$), as well as an interaction between age, sleep condition, and trial ($Fw(3) = 0.82$; $p < 0.05$). Analysis of simple effects showed that context cells in YCs and OSD mice were more stable than in OSD animals (OC versus OSD: $Tw(7.30) = 2.82$, $p < 0.03$; YC versus OC: $Tw(7.38) = 3.31$, $p < 0.02$). Interestingly, there was no difference between YCs and YSD mice in the stability of context cells ($Tw(20.06) = 1.03$; $p = 0.32$; Figure 3B), suggesting that the memory impairment observed in the latter was not due to a failure in recalling the environment.

We also hypothesized that, if animals noticed the change in object position during the test, object configuration cells should display remapping. However, if animals failed to notice the moved object, these cells should remain stable. Object configuration cells displayed effects of age ($Fw(1) = 18.71$; $p < 0.0001$), trial ($Fw(3) = 24.30$; $p < 0.0001$), an interaction between age and trial ($Fw(1) = 3.88$; $p < 0.0001$), and a trend in the interaction between sleep condition and trial ($Fw(3) = 0.68$; $p < 0.06$). Based on our definition of object cells, analysis of simple effects showed that all the groups displayed remapping between Hab and T1 ($Zw = 12.52$; $p < 0.00001$) and, as expected, between T3 and test ($Zw = 7.31$; $p < 0.0001$). Importantly, successful memory performance in YCs and OSD was associated with similar levels of object cell remapping. Moreover, object cells in YSD animals displayed more stability than those in OSD mice during the test ($Tw(59.48) = 4.34$; $p < 0.0001$; Figure 3C). Finally, there were no stability differences in unstable cells across groups or trials (age:

Fw(1) = 0.35, p = 0.56; sleep: Fw(1) = 0.76, p = 0.51; trial: Fw(3) = 0.76, p = 0.52; age versus sleep versus trial: Fw(3) = 0.43, p < 0.73; Figure 3D). Together, these data indicate that the successful memory performance observed in YCs and OSD mice is associated with stable context cells and flexible object configuration representations.

To evaluate whether the remapping observed in YC and OC animals reflected different mnemonic processes, the former being associated with memory updating and the latter reflecting typical long-term instability, we conducted an unmoved object control task in a subset of animals. Three young mice (30 cells) and four old mice (24 cells) were trained in the OPR task and allowed to sleep *ad libitum* during post-learning and recovery. However, during the test, all objects remained in the same position (Figure 4A). We found no significant differences in cluster quality in YC and OC cells (Figure 4B; isolation distance: age Fw(1) = 0.44, p = 0.51; trial: Fw(4) = 1.17, p = 0.35; interaction between age and trial: Fw(4) = 0.20, p = 0.94; see Figures S3 for L-ratio statistics). Then, we examined the stability patterns of context, object configuration, and unstable cells. As expected, the short-term stability of context and object configuration cells during training was higher than their long-term stability (context: trial: Fw(3) = 7.97, p < 0.04; T2/T3 versus T3/test: Zw = 0.75, p < 0.04; object configuration: trial: Fw(3) = 13.37, p < 0.004; interaction age and trial Fw(3) = 4.85, p < 0.04). Critically, both types of cells were more stable in young mice than in old mice during the test (context: Tw(5.73) = 3.49, p < 0.02; Figure 4C; object configuration: Tw(6.83) = 4.75, p < 0.003; Figure 4D). Unstable cells displayed similar remapping characteristics in both groups across all trials (p > 0.05; Figure 4E). These data indicate that the remapping observed in YC mice during the moved object test reflects memory updating rather than passage of time, and the high instability of object cells in OCs is inherent in this group.

Sleep analysis: Bayes classifier validation

Sleep patterns from young an old animals were recorded in chambers that provided free access to food and water (Figures S4A). To analyze the wake and sleep periods, we used a validated Bayes classifier to minimize inter-observer variability (Grigg-Damberger, 2012). This classifier has been previously tested in young and old mice (Rytkönen et al., 2011). To visualize the accuracy of the classifier in our dataset, we color coded the EMG and EEG using the output of the Bayes classifier to determine that there were no significant errors in the scoring of wake, NREM, and REM states (Figure S4B). Then, we partially re-validated this method comparing manual visual scoring with the output of Bayes classifier. A confusion matrix was created for each animal, and an average matrix was generated by averaging values for each age group (4 young and 4 old mice; Figures S4C and S4D). Accuracy was calculated by adding the values in which algorithm and visual scoring correlated in wake, NREM, and REM divided by the total entries (Figure S4E). Then, we calculated sensitivity (true positive rate) and specificity (true negative rate) for both young and old animals to generate a receiver-operating curve (ROC). The classifier generated outputs with high positive rates and minimal false positives (Figure S4F). Together, the results indicated that the algorithm was very accurate for both young and old mice. Moreover, we compared the reliability of the classifier using 5% and 10% of

manually scored data, obtaining highly similar results (average inter-score correlation: 95% ± 0.54%; 3 mice).

OC mice display more fragmented NREM sleep patterns than young mice during post-learning *ad libitum* sleep

We analyzed sleep patterns in YCs and OCs during the post-learning *ad libitum* sleep period (young: n = 9 [2 mice were not included due to noise in the recordings]; old: n = 8). We found that the total percent time spent in wake, NREM, and REM was equivalent in YC and OC animals (wake: $Tw(10.33) = 0.91$, $p = 0.39$; NREM: $Tw(10.47) = 0.49$, $p = 0.63$; REM: $Tw(10.28) = 1.42$, $p = 0.19$; Figure 5A). However, old animals displayed more NREM and REM bouts and a non-significant increase in wake bouts than young controls (NREM: $Tw(9.23) = 2.84$, $p < 0.02$; REM: $Tw(8.46) = 2.97$, $p < 0.02$; wake: $Tw(6.75) = 1.37$, $p = 0.22$; Figure 5B). Additionally, old mice displayed a trend toward shorter wake and NREM bout length than young controls (wake: $Tw(9.85) = 1.92$, $p = 0.09$; NREM: $Tw(10.97) = 2.09$, $p = 0.06$) but no differences in REM bout length (REM bout length: $Tw(10.54) = 1.01$; $p = 0.34$; Figure 5C). These results indicate that old animals display more fragmented NREM sleep than young mice, as previously observed (Pace-Schott and Spencer, 2015).

Next, we analyzed sleep patterns in the SD groups during the first 5 h post-learning to corroborate that the animals remained awake during this period. On average, SD mice were awake 97.5% of the time (young: 97.55% ± 1.26%; old: 97.51% ± 1.59%; data not shown), indicating that the SD procedure was effective.

Old and young mice display increased NREM bout length during recovery sleep following SD

Following the initial 5-h post-training period, we recorded 5 additional h of *ad libitum* sleep in the control and SD groups to evaluate the effects of SD on recovery sleep (YC: n = 11; YSD: n = 11; OC: n = 8; OSD: n = 10). Old and young animals did not display differences in total time spent in wake or REM (wake: age: $Fw(1) = 0.33$, $p = 0.57$; sleep: $Fw(1) = 3.02$, $p = 0.10$; age versus sleep: $Fw(1) = 0.04$, $p = 0.85$; REM: age: $Fw(1) = 0.84$, $p = 0.36$; sleep: $Fw(1) = 0.76$, $p = 0.39$; age versus sleep: $Fw(1) = 0.08$, $p = 0.68$; Figure 5D). However, there was an effect of sleep condition in NREM ($Fw(1) = 4.65$; $p < 0.05$) but no age or interaction effects (age: $Fw(1) = 0.09$, $p = 0.77$; age versus sleep: $Fw(1) = 0.06$, $p = 0.74$), which reflected that both YSD and OSD animals displayed more time in NREM (Figure 5D).

Next, we analyzed changes in sleep microstructure during wake, NREM, and REM. There were no significant changes in wake bout numbers or length (bout number: age: $Fw(1) = 1.23$, $p = 0.28$; sleep: $Fw(1) = 1.99$, $p = 0.18$; age versus sleep: $Fw(1) = 0.05$, $p = 0.82$; bout length: age: $Fw(1) = 0.40$, $p = 0.54$; sleep: $Fw(1) = 0.02$, $p = 0.90$; age versus sleep: $Fw(1) = 0.01$, $p = 0.97$; Figures 5E and 5F). Conversely, there was an effect of sleep condition ($Fw(1) = 5.34$; $p < 0.05$) and an interaction between age and sleep condition in NREM bout number ($Fw(1) = 0.32$; $p < 0.04$). Analysis of this interaction showed that OSD mice displayed fewer NREM bouts than OCs ($Tw(5.66) = 2.73$; $p < 0.04$), but there were no differences between the young groups ($Tw(8.88) = 1.04$; $p = 0.33$; Figure 5E). Additionally,

there was an effect of sleep condition in NREM bout length, reflecting that both YSD and OSD groups displayed longer NREM bouts than controls ($Fw(1) = 7.53$; $p < 0.02$; Figure 5F). The observation that OSD mice displayed fewer numbers of NREM bouts of longer length than OCs indicated that NREM was consolidated in this group.

Finally, there was an interaction between age and sleep condition in the number of REM bouts ($T_W(1) = -0.36$; $p < 0.05$; Figure 5E), but these differences were modest and did not reach significance in post hoc tests (number of bouts: YC versus YSD: $Tw(9.56) = 1.41$, $p = 0.19$; OC versus OSD: $Tw(9.83) = 0.84$, $p = 0.37$). Differences in REM bout length were also not significant ($p > 0.05$; Figure 5F), suggesting that 5 h of SD only produce subtle changes in REM. In summary, these data indicate that acute SD serves to increase NREM bout length in both young and old mice, further decreasing NREM bout number in old mice. These changes may serve to consolidate the typical fragmented NREM sleep observed in old mice.

Acute SD increases relative delta power (RDP) during NREM and decreases relative theta power (RTP) during REM in SD mice

Because delta (0.25–4 Hz) and theta (4–10 Hz) oscillations have been associated with attention, spatial exploration, and memory (Hasselmo, 2006; Hutchison and Rathore, 2015), we investigated whether the power of these bands was differentially altered during the SD period and/or during subsequent *ad libitum* sleep periods. We found no differences in RDP or RTP during SD (RDP: YSD ($n = 11$): 0.12 ± 0.01; OSD ($n = 10$): 0.11 ± 0.02; RTP: YSD: 0.41 ± 0.04; OSD: 0.39 ± 0.06; $p > 0.05$; data not shown), indicating that the movement of the bar did not differentially affect the EEG in the experimental groups.

We then generated average power spectra during NREM and REM in post-learning (Figures 5G, 5H, S5A, and S5B) and recovery sleep (Figures 5I, 5J, and S5C-S5F). Power spectra displayed peaks at low frequencies (3 to 4 Hz) during NREM and medium frequencies (7 to 8 Hz) during REM, corresponding to delta and theta frequency bands, respectively. There were no significant differences in RDP during NREM ($Tw(9.63) = 0.87$; $p = 0.41$; Figure 5K) or RTP during REM ($Tw(5.59) = 1.02$; $p = 0.35$; Figure 5L) between YC and OC mice during the *ad libitum* post-learning sleep period. RDP showed an effect of sleep condition during recovery ($Fw(1) = 9.40$; $p < 0.007$; Figure 5M), reflecting an increase in both YSD and OSD animals, as previously shown (Halassa et al., 2009). However, there were no differences in RTP (age: $Fw(1) = 0.26$, $p = 0.62$; sleep: $Fw(1) = 0.30$, $p = 0.59$; interaction between sleep and age: $Fw(1) = 0.33$, $p = 0.10$; Figure 5N). Finally, we also examined relative sigma (10–15 Hz) and beta (15–25 Hz) power during post-learning and recovery, finding no significant differences between the groups ($p > 0.05$; Figures S5G-S5J). In summary, these data suggest that 5 h of SD followed by 5 h of recovery sleep do not result in age differences in relative power.

YC mice display more spindles of longer length than OC mice immediately following training

Spindles may play a role in memory consolidation by facilitating memory reactivation (Rasch and Born, 2013). We quantified spindle characteristics using a highly accurate

automated spindle-detection method (Uygun et al., 2019). First, we performed a partial re-validation of the method obtaining 95% reliability (n = 4; young: 97% overall correlation; old: 94% overall correlation). Errors included 2.5% of false positives and 2% of false negatives. Moreover, we color coded the detected spindles in the filtered EEG to visually inspect the reliability of the code (Figure 6A), observing very accurate results.

Using this method, we analyzed spindles during NREM periods. There were no significant differences in average number, frequency, or duration of spindles between young and old control mice during the *ad libitum* post-training sleep period (spindle count: $Tw(10.99) = 0.52$, $p = 0.62$; spindle duration: $Tw(9) = 0.004$, $p = 0.99$; spindle frequency: $Tw(8.19) = 0.01$, $p = 0.99$; Figures 6B-6D). Because the initial hours following training have been shown to be critical for memory consolidation in young-adult animals (Bailey et al., 2004; Palchykova et al., 2006), we divided the post-training sleep period into consecutive 1-h segments to investigate whether there were differences at distinct stages. We found a significant main effect of segment and an interaction between age group and segment in spindle numbers (segment: $Fw(4) = 8.73$, $p < 0.008$; interaction: $Fw(4) = 4.35$, $p < 0.05$). Analysis of simple effects indicated that YC animals displayed more spindles than OCs during the 1st h post-learning ($Tw(10.06) = 4.18$; $p < 0.002$; Figure 6B). No differences in spindle duration or frequency were observed in the segment analysis (spindle duration: age: $Fw(1) = 0.06$, $p = 0.82$; hour: $Tw(4) = 0.64$, $p = 0.65$; age versus hour: $Tw(4) = 1.15$, $p = 0.41$; spindle frequency: age: $Fw(1) = 0.22$, $p = 0.65$; hour: $Tw(4) = 0.81$, $p = 0.64$; age versus hour: $Tw(4) = 0.34$, $p = 0.89$; Figures 6C and 6D). These results indicate that high number of spindles early during post-learning sleep may facilitate memory consolidation in young mice.

An acute session of SD increases total number of spindles in old animals during recovery

Previous research indicated that the time window for memory consolidation is extended or delayed in old animals in comparison to young ones (Schimanski and Barnes, 2010). These findings suggest that increases in spindle count occurring even several hours following learning may have a significant impact on memory consolidation in old animals. To test this idea, we examined spindle count, duration, and frequency during the recovery *ad libitum* sleep period following SD. We found a significant interaction between age group and sleep condition on spindle count ($Fw(1) = 1.00$; $p < 0.02$). Analysis of single effects revealed that OSD mice displayed more spindles than OCs ($Tw(8.85) = 3.29$; $p < 0.01$) and YSD mice ($Tw(9.37) = 4.77$; $p < 0.001$; Figure 6E). There were no differences in spindle duration during recovery (age: $Fw(1) = 0.23$, $p = 0.64$; sleep: $Fw(1) = 0.30$, $p = 0.59$; age versus sleep: $Fw(1) = 1.0$, $p = 0.66$; Figure 6F), but there was an interaction between age and sleep condition on spindle frequency ($Fw(1) = 0.37$; $p < 0.05$). This effect was driven by YSD animals displaying higher spindle frequency than old mice ($Tw(10.29) = -3.73$; $p < 0.004$; Figure 6G), a characteristic previously observed in adult humans following SD (Rosinvil et al., 2015).

We then examined whether there were differences in spindle characteristics across the groups at different times during recovery by subdividing this period into 1-h segments. We found a significant effect of segment ($Fw(4) = 0.90$; $p < 0.009$; Figure 6E) but no

interactions ($p > 0.05$). Analysis of single effects indicated that spindle counts during the last segment were higher than the preceding one ($Zw = 3.05$; $p < 0.03$; Figure 6E). There were no significant effects of segment, sleep, or interactions in spindle duration or frequency (spindle duration: sleep: $Fw(1) = 0.01$, $p = 0.97$; hour: $Fw(4) = 0.37$, $p = 0.83$; age versus sleep versus hour: $Fw(4) = 0.08$, $p = 0.99$; spindle frequency: sleep: $Fw(1) = 0.01$, $p = 0.96$; hour: $Fw(4) = 0.17$, $p = 0.96$; age versus sleep versus hour: $Fw(4) = 0.09$, $p = 0.99$; Figures 6F and 6G). In summary, the spindle analysis revealed that there is a sustained increase in average number of spindles in OSD mice in comparison to OCs during recovery, which may serve to consolidate memory.

Because spindles are more prominent during NREM/REM transitions (Uygun et al., 2019), we also plotted sigma power during NREM/REM transitions and corroborated that our groups displayed the typical power shift (Figures 7A-7F). Sigma power increased during NREM prior to the transition and decayed rapidly at the onset of REM, as previously shown in mice (Uygun et al., 2019; Winsky-Sommerer et al., 2008; post-learning: Figures 7A and 7B, $Fw(1) = 52.85$, $p < 0.00001$; recovery: Figures 7C-7F, $Fw(1) = 259.31$, $p < 0.00001$). We did not observe significant differences between young and old mice when we evaluated spindles during post-learning transitions, which parallels the absence of differences in average spindle count during this period, i.e., the differences were only observed during the 1st h post-learning (Figure 7G; age: $Fw(1) = 0.94$, $p = 0.39$; interaction age versus transition phase: $Fw(1) = 0.26$, $p = 0.60$). However, YC and OSD animals displayed more spindles than YSD mice during sigma transitions occurring during recovery (Figure 7H; interaction between sleep and age: $Fw(1) = 4.38$, $p < 0.05$; YC versus YSD: $Tw(17.24) = 2.70$, $p < 0.02$; OSD versus YSD: $Tw(1) = 2.55$, $p < 0.02$).

Finally, to determine whether the number of spindles occurring 60 s prior to the NREM/REM sigma transitions were associated with performance, we calculated correlations between these measures. In all cases, regardless of whether, on average, the groups displayed OPR memory or not, we observed positive correlations between performance and spindle counts. However, the correlations reached significance for the YCs post-learning, as well as the OSD and YSD group during recovery ($p < 0.05$; Figures 7I-7L). These results indicate that spindle counts immediately prior to NREM/REM transitions are a good predictor of memory.

DISCUSSION

In this study, SD impaired OPR memory in young adult mice but unexpectedly enhanced performance in old mice. Successful OPR memory in YCs and OSD mice was associated with stability of context cells representing the static aspects of the context and remapping of object configuration cells coding the arrangement of the objects within the context. Although NREM bout length increased in both YSD and OSD groups, the latter group also exhibited fewer NREM bouts during recovery, suggesting a reduction in NREM fragmentation typically observed in old subjects. Improved memory performance was also associated with high spindle counts early during post-learning sleep in YCs and an increase in average spindle counts during recovery in OSD mice. Notably, spindle counts during NREM/REM sigma transitions were a good predictor of performance, especially for YCs

during post-learning sleep and SD groups during recovery. These data indicate that SD has differential effects in young and old mice. We suggest that acute SD produces changes in sleep microarchitecture that serve to ameliorate age-related cognitive deficits and improve the flexibility and stability of hippocampal representations.

Sleep fragmentation has been associated with impaired memory consolidation (Sportiche et al., 2010; Tartar et al., 2006; Ward et al., 2009a, 2009b). Because memory traces are reactivated during NREM, a phenomenon thought to be crucial for consolidation (Abel et al., 2013; Rasch and Born, 2013), reducing NREM fragmentation may be advantageous for cognitive function. However, NREM consolidation may not be sufficient to enhance memory because YSD animals also display longer NREM bouts but poor OPR performance. Strong evidence links spindles with memory consolidation (Antony et al., 2019; Ulrich, 2016), and alterations in spindles are good predictors of age-related cognitive decline (Taillard et al., 2019). Therefore, the enhanced memory performance observed in OSD animals may be due to both improved NREM sleep quality and increases in spindle counts during recovery. Interestingly, YSD mice not only displayed low spindle counts but also an increase in spindle frequency during recovery sleep. Although the significance of spindle frequency in rodents remains to be determined, studies in children found that high spindle frequencies show negative correlations with cognitive abilities, whereas low ones show the opposite results (Chatburn et al., 2013; Geiger et al., 2011). These findings suggest that performance deficits in YSD mice could also be related to changes in spindle frequency.

How are spindles connected to hippocampal memory consolidation? One of the most prevalent theories suggests that memories are simultaneously formed in hippocampus and cortex (Preston and Eichenbaum, 2013). Following learning, additional crosstalk between these regions is necessary to strengthen the cortical engrams (Squire et al., 2015). In the hippocampus, patterns of neuronal activity are replayed during NREM sharp wave ripples (Buzsáki, 2015; Joo and Frank, 2018). Additionally, spindles generated in the thalamic reticular nucleus are also relayed to cortex during NREM (Contreras et al., 1996). Because cortical spindles are associated with increased dendritic activity (Seibt et al., 2017) and intracellular calcium (Niethard et al., 2018), their activity may serve to initiate plastic changes involved in cortical memory consolidation (Peyrache and Seibt, 2020). Critically, spindles serve to organize hippocampal replay during sharp waves (Varela and Wilson, 2020), a phenomenon that likely facilitates hippocampal memory consolidation. In this context, the increase in spindle activity observed in OSD animals during recovery may facilitate mnemonic function by enhancing replay.

It was previously thought that the stability of place cells was critical for memory (Kentros et al., 2004; Muzzio et al., 2009a). However, recent findings in mice found that hippocampal cells expressing cfos, an activity marker associated with the formation of memory engrams (Liu et al., 2014), are much more unstable than cells that do not express this early gene (Tanaka et al., 2018). This confirms that subsets of cells participating in memory processes are unstable. Furthermore, unstable subpopulations coexist with stable ones, potentially having distinct mnemonic functions. These observations are in line with our finding suggesting that instability of object configuration cells is important for memory updating, whereas stability of context cells likely reflects coding of static contextual aspects.

A previous OPR study in young adult rats allowed to sleep *ad libitum* showed that hippocampal CA1 neurons exhibited changes in firing rate, but not in the cells' preferred firing locations, during the moved-object test (Larkin et al., 2014). Similarly, we observed rate remapping during the moved-object test in YC and OSD mice. However, we also found that successful learning was associated with place-field remapping in a subset of CA1 neurons. The differences in stability between our observations and Larkin et al. may be related to the intrinsic differences between mice and rats (Kentros et al., 2004; Muzzio et al., 2009b) and/or the different retention intervals used in these studies (5 min in Larkin et al. compared to ≥15 h in our study). In future studies, it will be important to determine whether SD also affects remapping in other tasks and/or improves the long-term stability of object configuration cells when objects are unmoved.

Other studies using the OPR task in young adult animals found that immediate post-training sleep is critical for memory. Performance is optimal when the retention interval occurs during the inactive light phase and animals are allowed to sleep (Binder et al., 2012), whereas impaired OPR memory is consistently observed following post-training SD (Havekes et al., 2014; Prince et al., 2014; Sawangjit et al., 2018). Although these behavioral deficits have been attributed to complete disruption of memory consolidation, our results suggest otherwise. The long-term stability of context cells in YSD mice suggests that static representations of the environment are retrieved correctly, but the lack of remapping of object configuration cells suggests that the object arrangement is not properly updated. This interpretation is corroborated by the fact that YC mice do not show object cell remapping when the configuration remains stable (i.e., unmoved control task). The synaptic homeostasis hypothesis proposed by Tononi and colleagues posits that, rather than actively strengthening memories, sleep may instead serve to downscale synapses in order to allow further memory acquisition (Tononi and Cirelli, 2006). Our results suggest that, in young adult animals, SD may interfere with this process by making hippocampus-dependent representations more rigid and less flexible. Thus, the lack of remapping in response to environmental changes may reflect incomplete downscaling of synapses, which prevents correct encoding of a new object configuration. This idea is supported by observations showing that place cell remapping involves plastic mechanisms associated with synaptic depression (Schoenenberger et al., 2016).

Similarly to YSD mice, OC animals showed deficits in OPR performance, corroborating previous findings (Wimmer et al., 2012). However, hippocampal representations are different in these groups: context cells are stable in YSD mice, but not in OCs. Place cell instability in old animals has been previously reported (Barnes et al., 1997), along with impairments in several spatial tasks (Rosenzweig and Barnes, 2003) and sleep fragmentation (Wimmer et al., 2013). Our data suggest that age-related sleep fragmentation contributes to impaired consolidation of the static aspects of the environment.

It is well established that, in young adult animals, the initial hours after training are critical for initiating transcriptional events leading to the translation of new proteins important for memory consolidation (Bailey et al., 2004). Our data support this idea by showing that SD impairs young adults when it happens immediately following learning, but not when it is delayed 5 h after training, as previously shown (Palchykova et al., 2006). Interestingly,

it is thought that protein-synthesis-mediated consolidation is extended and/or delayed in old animals (Schimanski and Barnes, 2010). Moreover, it was shown that SD inhibits translational processes in young mice, but not in old ones (Naidoo et al., 2008), further suggesting that consolidation processes are different in old animals. Our data showing increases in spindle counts and enhanced OPR performance in OSD mice appear to corroborate this idea. Because mnemonic advantages in old animals disappear when SD happens 5 h after training, it is likely that the time window for consolidation in this group also has boundaries. Alternatively, delayed SD may not be beneficial because it pushes recovery sleep to the beginning of the dark cycle, when rodents are normally active, making the process more ineffective.

Increased delta power has been reported following SD (Davis et al., 2011). However, this effect depends on the duration of wakefulness (Dispersyn et al., 2017; Halassa et al., 2009), animal housing conditions (Kaushal et al., 2012), and several other variables (Davis et al., 2011). In our experiments, SD produced an increase in RDP in SD animals but no age differences. Other studies using similar normalization methods reported age-dependent increases in RDP (Mendelson and Bergmann, 1999; Panagiotou et al., 2017). These discrepancies may reflect differences in procedures, including length of SD (48 h versus 5 h) or recovery period (24 h versus 5 h) and/or evaluation of RDP at distinct times of the sleep cycle. For example, old rats display higher RDP than young ones only during the first part of the dark cycle (Mendelson and Bergmann, 1999). We evaluated RDP during the second half of the light phase, following training and SD. Therefore, our results do not contradict previous reports but rather highlight the effects of distinct analysis times and/or procedures.

In summary, our findings contribute to a better understanding of the effects of sleep quality on memory and hippocampal representations and have potential clinical implications for rescuing age-related cognitive deficits.

STAR★METHODS

RESOURCE AVAILABILITY

Lead contact—Further information and requests for resources and/or code should be directed to and will be fulfilled by the Lead Contact, Isabel Muzzio (isabel.muzzio@utsa.edu)

Materials availability—This study did not generate new unique reagents.

Data and code availability—The code generated during this study is available in GITHUB. Tetrode and sleep datasets are uploaded in Mendeley.

EXPERIMENTAL MODEL AND SUBJECT DETAILS

Mice—Young and aged adult male C57BL/6J mice (Jackson Laboratory, Bar Harbor, ME) were housed individually on a 12-hour light/dark cycle and allowed access to food and water *ad libitum*. The age range of animals implanted with EEG headstages and EMG wires was 10-14 weeks old for young and 60-64 weeks old for old mice. For tetrode recordings, it was

10-24 weeks old for young and 60-76 weeks old for old. The wide age range in the latter group reflected the fact that positioning tetrodes in the cell body layer and optimization of recording stability required a different time frame from animal to animal.

The age range of animals implanted with EEG headstages and EMG wires was 10-14 weeks old for young and 60-64 weeks old for old mice. For tetrode recordings, it was 10-24 weeks old for young and 60-76 weeks old for old. The wide age range in the latter group reflected the fact that positioning tetrodes in the cell body layer and optimization of recording stability required a different time frame from animal to animal. Animal living conditions were consistent with the standard required by the Association for Assessment and Accreditation of Laboratory Animal Care (AAALAC). All experiments were approved by the Institution of Animal Care and Use Committee of the University of Texas at San Antonio and were carried out in accordance with NIH guidelines.

METHOD DETAILS

Surgery—For sleep recordings, prefabricated 2 EEG and 1 electromyograph (EMG) channel headmounts (Pinnacle Technology) were implanted [from Bregma (in mm): frontal leads: AP: +3.2, ML: ± 1., and parietal leads: AP: −1.8, ML: ± 1.2] and secured with cyanoacrylate and dental cement. Two EMG leads were placed under the nuchal musculature and affixed with VetBond. For place cell recordings, animals were implanted with custom made drivable six-tetrode microdrives made in our laboratory using Neuralynx connectors (EIB-36-narrow). The microdrives were affixed to the skull with cyanoacrylate and dental cement, with recording electrodes placed directly above the dorsal hippocampus [from Bregma (in mm): AP, −1.7; ML, −1.6; form dura; DV, −1.0]. A ground wire was connected to a screw placed on the contralateral side of the skull. Tetrodes were made with 0.25 μm insulated wires (California Fine Wire, Grover beach, CA) with impedance values ranging 300-600 KΩ at 1 kHz (1-1.5 KΩ before plating). Animals underwent at least one week of recovery prior to recordings.

Sleep deprivation (SD)—An automated SD cylindrical apparatus (Pinnacle Technology, Lawrence, KS) containing a bar spanning the enclosure was used for all SD procedures. Animals were individually housed in the apparatus for at least 24 hours prior to the beginning of the experiments with fresh bedding, food, and water, and were returned to the apparatus in between trials. To induce SD, the bar was rotated continuously by a motor at approximately 3 rpm with random reversals in rotational direction to prevent subjects from acquiring brief sleep periods through adaptation to the pattern of rotation. A trained experimenter verified visually that the bar rotated at all times and that mice did not use any alternative strategies to sleep.

Behavioral training—For all animals, behavioral procedures (e.g., exposure to the objects on day 1 and memory testing on day 2) were conducted during the first 4 hr of the light cycle (ZT 0-4). All animals were exposed to either SD or *ad libitum* sleep periods immediately following training. The object/place recognition task (OPR) was conducted in a square context (35cm x 35cm) with visual features on each wall for orientation (Figure 1A). Everyday items (glass beer bottle, metal soda can, and plastic juice bottle) were used as

objects after pilot testing determined that on average mice showed roughly equal preference for all items. On day 1, animals were habituated to the empty context for a 6 min habituation trial (Hab). After the habituation, the 3 objects were arranged along one of the diagonal axes of the context and three 6-min object exploration trials (T1-3) were conducted. During the inter-trial interval (2 min), the animals were placed in their home cage and the context and objects were wiped down with 70% ethanol. Immediately following the third object trial (T3), animals in the experimental groups were housed in the experimental chamber and were SD for 5 hr, whereas controls were housed in the same chamber but allowed to sleep. On day 2, one object was moved from its original location to an adjacent corner and mice were tested for 6 min in the context with the moved object (Test). In the delayed SD procedure, animals were also trained as described above and allowed to sleep *ad libitum* for 5 hr following training before undergoing the delayed 5 hr SD, followed by 5 hr of recovery sleep. In the unmoved object control condition, animals were trained as described for the traditional OPR and allowed to sleep *ad libitum* following training, but all objects remained in their original locations during the test. In all conditions object positions were counterbalanced across trials.

Behavioral analysis—All object exploration trials were video recorded using Limelight (Actimetrics, Wilmette, IL) and analyzed offline by researchers blind to the group condition. All instances when an animal was oriented toward and touching an object with nose, vibrissae, and/or forelegs within 0-3 cm of the object were recorded as “object exploration”; contacting an object while passing or oriented away were not considered. Animals with an average object exploration time less than 10 s were excluded from analysis (2 mice were excluded due to poor exploration). Behavioral data from animals used for sleep analysis was combined with data from animals used for place cell recordings.

Object preference was calculated as the percentage of time spent exploring the moved object in the test session relative to total object exploration time during testing minus the relative time exploring the same object during training, as previously described (Oliveira et al., 2010). This formula estimates object preference taking into account any potential object bias that animals may have during training:

$$\%\ change\ in\ preference = 100 * \left(\frac{moved\ object\ exploration_{test}}{total\ object\ exploration_{test}} - \frac{moved\ object\ exploration_{trial\ 1-3}}{total\ object\ exploration_{trian\ 1-3}} \right)$$

A larger percentage change indicates greater preference for the moved object during the test session, while lower values indicate little change in preference from day 1 to day 2, after the object is displaced. To rule out novelty effects, we repeated the same analysis excluding trial 1 when the objects were first introduced. To calculate preference for the unmoved objects we used the following formula, but replaced the numerator of the second term in the equation with the time spent exploring the unmoved object.

Plasma corticosterone measures—Young and old animals were randomly assigned into control and experimental conditions between 8-10 AM. The experimental animals were SD for 5 hours, whereas control mice were allowed to sleep *ad libitum* in the experimental chamber. Following this period, all animals were deeply anesthetized with

a mixture of ketamine and xylazine (100/10 mg/kg) and blood samples were extracted by cardiac puncture. Plasma was frozen and sent to Penn Diabetes Center Radioimmunoassays and Biomarkers Core for analysis (University of Pennsylvania, Philadelphia, PA). Blood collection was conducted during the second quarter of the light cycle between 2-4 PM for all animals.

Place cell recordings and analysis—Beginning 1-2 weeks after surgery, neural activity was screened daily in an environment different from the context used for experiments, advancing the electrode bundle 5-10 μm per day until pyramidal cells could be identified by their characteristic firing patterns (Ranck, 1973). Lowering the electrodes in small steps minimizes electrode drift and ensures recording stability for several days (Muzzio et al., 2009b; Wang et al., 2012). Additionally, all animals yielding unit data remained connected to the recording setup via a commutator until the end of the experiment to further minimize the possibility of electrode drift through plugging/unplugging. Long-term recordings were considered stable when cells had the same cluster boundaries over two sessions (at least 24 hr apart), and the waveforms obtained from all four wires of a tetrode were identical. Experiments only began when recordings were stable for 24 hr. Animal position and electrophysiological data were recorded using Cheetah Data Acquisition system (Neuralynx, Bozeman, MN), as previously described (Wang et al., 2012, 2015).

Units were isolated using MClust software (developed by A. David Redish, University of Minnesota) and accepted for analysis only if they formed isolated clusters with clear Gaussian ellipses and minimal overlap with surrounding cells and noise. All cells were inspected to rule out the presence of events during the 2 ms refractory period. Place field maps were generated using custom MATLAB code as previously described (Keinath et al., 2014; Wang et al., 2012,2015). Briefly, the arena was first divided into a 20x20 pixel grid and activity maps (the total number of spikes in each pixel) and sampling maps (the total amount of time spent in each pixel) were computed. Both maps were then smoothed with a 3 cm Gaussian kernel. The smoothed activity map was then divided by the smoothed sampling map, which yielded the place field map. Any location sampled for less than 1 s was considered un-sampled. Only periods of movement were included in the analysis (minimum walking speed: 2 cm/s). Cells that fired less than 25 spikes during movement or displayed peak firing frequencies below 1 Hz before smoothing were excluded from analysis. Firing rate patterns were characterized by computing the overall mean (MFR: total number of spikes divided by time spent in the arena), peak firing rate (PFR: maximum rate value), and out of field firing rate (OFFR: spikes occurring outside areas defined as place fields). Place fields were defined as any set of at least 9 contiguous pixels in which the average firing rate was at least 20% of the peak firing rate (Rowland et al., 2011). If a cell yielded multiple place fields, the sum of all fields was taken as the place field size. Rate remapping was calculated as the absolute difference between the peak firing rate of individual cells on consecutive trials. The spatial information content, a parameter that estimates how well the firing pattern of a given cell predicts the location of the animal, was computed as previously described (Skaggs et al., 1993) using the following formula $IC = \Sigma pi(Ri/R)\log(Ri/R)$,where pi is the probability of occupying location i, Ri is the firing rate at location i, and R is the overall mean firing rate.

Place field stability was assessed by calculating pixel-to-pixel cross-correlations between maps. The generated Pearson R correlation value reflected the degree of map similarity across trials for all cells. Overall global remapping was estimated by averaging the Pearson r correlation values across cells and animals in each condition. Additionally, cell types were classified into three categories depending on whether they remapped in the presence of the objects (object configuration cells), remained stable throughout training (context cells), or displayed both short- and long-term instability (unstable cells), with stability defined as a correlation value above 0.35, a threshold. This threshold was estimated using correlation scatterplots, distributions, and a machine learning algorithm (MATLAB *kmeans*) (Figures S3).

Isolation distance and L-ratio—Cluster quality was assessed by computing two metrics: isolation distance (ID, (Harris et al., 2001), and L-Ratio (Schmitzer-Torbert et al., 2005). Both measures use the Mahalanobis distance ($D^2_{i,C}$), which calculates the distance between points in a high dimensional space where dimensions are correlated. $D^2_{i,c}$ is calculated as follows:

$$D^2_{i,\,c} = (x_i - \mu_c)^T E_c{}^{-1} (x_i - \mu_c)$$

In this formula, x_i is the feature vector for spike i, μ_c is the mean of the of the distance values of the spikes in cluster c, E_c is the covariance matrix of the spikes in c. In all our calculations we incorporated spikes from other clusters as well as noise.

ID estimates how distant the cluster spikes are from other recorded spikes on the same tetrode. Thus, once Mahalanobis distances are calculated, the values are sorted closest to furthest. If a cluster contains N number of spikes, ID distance is the D^2 of the N^{th} closest noise spike. A high ID means that non-cluster spikes are located far away from the evaluated cluster, a low value means the opposite. The ID is not normalized against cluster size. As such, clusters with less spikes tend to have lower ID values than those with many spikes.

L-Ratio estimates how well cluster spikes are separated from other spikes recorded from the same tetrode. This calculation is based on the assumption that for Gaussian spike distributions, the Mahalanobis distance will follow a χ^2 with eight degrees of freedom (df). First, the parameter L is calculated as follows:

$$L - Ratio(c) = \frac{1}{n_c} \sum_{i \notin c} \left(1 - CDF\,\chi^2_{df}\left(D^2_{i,\,c}\right)\right)$$

In this formula, (i not in C) are the spikes that are not part of the cluster, CDF χ^2_{df} is the cumulative χ^2 distribution with 8 degrees of freedom. L-ratio is defined as L divided by the number of spikes in the cluster (n_c). A low L-Ratio indicates good cluster separation, a high L-Ratio the opposite.

Verification of tetrode placement—Tetrode placements were verified after completion of the experiments by passing a small current (0.1 mA) for 5 s through the tetrodes that

yielded data in anesthetized animals. The brains were removed and fixed in 10% formalin containing 3% potassium ferrocyanide for 24 hr. The tissue was cryosectioned and stained using standard histological procedures (Powers and Clark, 1955).

Sleep state analysis—EEG/EMG signals were recorded for 10 hours following training on day 1 (Pinnacle Technology, Lawrence, KS). The headmounts were attached to a preamplifier for first stage amplification (100x) and initial high-pass filtering (0.5 Hz for EEG and 10 Hz for EMG). All signals were then sampled at 400 Hz and digitized (Sirenia Acquisition software, Pinnacle Technology). Animals with excessive noise in any channels (> 10% of epochs classified as artifact) were discarded from analysis (2 animals were excluded from the post-training session due to noise and 2 animals were discarded from all sessions due to extremely noisy EEG and EMG).

Sleep recordings were divided into 4 s epochs. 5% of epochs were randomly selected for manual scoring with Sirenia Sleep analysis software using EMG power and EEG amplitude and frequency to categorize an epoch as a REM, NREM, or Wake states. Scoring randomly selected epochs produces more reliable outputs than continuous manual scoring of epochs (Rytkönen et al., 2011). The partially scored EEG/EMG files were then exported to MATLAB and the remaining epochs were analyzed using a naive Bayesian classifier, a highly accurate method that has been shown to produce inter-rater agreements of 92% (Rytkönen et al., 2011). The scoring method yielded total time, number of bouts, and bout length in wake, NREM, and REM. A bout was defined as a period of continuous epochs in a particular state.

Classifier validation—Complete visually scored data were compared with the output of the Bayes classifier to re-validate the method in a subset of animals. Additionally, outputs obtained with 5% and 10% manually scored inputs were compared to determine the effectiveness of the classifier using different amounts of input data in subsets of animals. To determine the accuracy, sensitivity and specificity of the classifier, a confusion matrix was created for each mouse visually scored. An experienced researcher visually scored 100% of the 4 s epochs comprising 5 hours of EEG and EMG activity. The researcher then selected only 5% of the epochs of the same recording. The 5% of visually scored epochs and the EEG and EMG recording were fed into the Bayes classifier to generated 5 hr of algorithm scored data. The scores from the researcher and classifier were then compared per epoch and added into the confusion matrix (y axis represents algorithm scoring and x axis visual scoring). Each entry of the confusion matrix was then divided by the total number of epochs and multiplied by 100 to turn the entries into percentages. An average confusion matrix was then computed for each age group (young and old, respectively). Confusion matrix measures:

a, e, and i (shown in gray in the diagram below) are the boxes that represent values in which algorithm and visual scoring coincided. Accuracy was calculated as follows:

$$\text{Accuracy} = (a + e + i)/(a + b + c + d + e + f + g + h + i)$$

$$\text{Wake Sensitivity (True Positive)} = a / (a + d + g)$$

Wake Specificity (True Negative) = (e + f + h + i)/(b + c + e + f + h + i)

NREM Sensitivity (True Positive) = e / (b + e + h)

NREM Specificity (True Negative) = (a + b + g + i)/(a + d + g+ c + f+i)

REM Sensitivity (True Positive) = i / (c + f + i)

REM Specificity (True Negative) = (a + b + d + e)/(a + b + d + e + g + h)

Where the entries of a confusion matrix are denoted as follows:

Algorithem Scorning (predicted)	Wake	a	b	c
	NREM	d	e	f
	REM	g	h	l
		Wake	NREM Visual scoring (Truth)	REM

Power spectra and relative band power—The average power spectra were calculated using wavelet analysis. The EEG time series was down sampled from a sampling rate of 400 Hz to 100 Hz and then the continuous wavelet transform (WT) was computed using the MATLAB command “cwt.” The resulting output was a matrix where columns represented time and rows frequencies. The wavelet power was computed by taking the absolute value of the wavelet transform. Since the frequency spacing of the continuous wavelet transform is not uniform (unlike the FFT), the power over a uniform frequency spacing was interpolated from 0.25 to 30.0 Hz in increments of 0.25 Hz. The relative band power was found by summing the power spectra over a band’s frequency range divided by the total power in a given state. The frequency bands were defined as follows: Delta: 0.25-4 Hz, Theta: 4-10 Hz, Sigma: 10-15 Hz, Beta: 15-25 Hz.

Spindle detention—Spindle detection during NREM was computed using a validated automated system for rapid and reliable detection of spindles using mouse EEG. This method eliminates observer bias and allows quantification of sleep parameters including count, duration, and frequency as well as rapid quantification during selective sleep segments. Briefly, the raw EEG signal was bandpass filtered using the *designfilt* MATLAB function, which was then applied to filter the data using *the filtfilt* function with the following parameters: First stopband frequency = 3 Hz, first passband frequency = 10 Hz, second passband frequency 15 Hz, second stopband frequency = 22 Hz, with stopband attenuation levels of 24 dB. Once the EEG was filtered, the root-mean squared of the signal was calculated using a 750 ms window to smooth the data. This window was selected to minimize erroneous detection of artifacts. The RMS values were then cubed to enhance separation of signal and noise. Finally, spindles were detected using a two-threshold approach that sets values from the mean cubed RMS transform of the NREM state. The lower threshold was calculated as 1.2 x mean cubed RMS and the upper threshold as 3.5 x mean cubed RMS (Uygun et al., 2019).

NREM/REM sigma transitions—Each EEG recording was processed individually. The sleep state scored data were used to compute the mean and standard deviation under Wake. These values were then used to z-score the remaining EEG data (all states). The data were down sampled from 400 to 100 Hz. The continuous wavelet transform was then computed, and its absolute squared value was calculated. Frequencies from 0.25 to 30.0 Hz were interpolated in increments of 0.25 Hz. Sigma power over time was computed by summing the spectrum over the sigma band (10-15 Hz) (regardless of state). The scored data were then used to compute the mean sigma power (across the entire recording) of only NREM epochs. The sigma power series was divided by the mean sigma power for normalization. The score data were used to detect all instances of NREM to REM transitions, and 60 s of normalized sigma power were selected before and after each transition (120 s total). The average NREM to REM sigma power transition time series was then computed by summing up all transitions and dividing by the total number of transitions for each mouse and an average for each age group and sleep condition was generated.

Spindle counts during sigma transitions—The average NREM to REM sigma power transition time series were separated into 3 s windows and numbers of spindles (calculated as stated above) were added for comparison across groups and correlations with OPR performance.

QUANTIFICATION AND STATISTICAL ANALYSIS

Since the experimental data had irregular variability, e.g., some data did not fulfill the homoscedasticity assumption, we opted for robust statistical analysis, in order to protect the findings against such problems (Wilcox, 2012). Therefore, all the results obtained through experiments are summarized in a Box-Plot graph according to robust statistics. All statistical details are provided in Data S1. For all tests, p values are noted in the last column of each Table.

For all the behavioral and EEG/EMG implanted animals, the N represented the number of animals in each group. For tetrode recordings, the N represented the number of cells. In all cases the numbers of animals and cells are noted in the Figure legends and results. For all experiments, p level was set using an alpha level of 0.05. For tetrode recordings, criteria for exclusion included poor sampling of the arena below 75% of the total area (1 young mouse was excluded). For EEG/EMG recordings, criteria for exclusion included extreme noise in the EEG or EMG wire (2 old animals were excluded in the post-learning session), or unattachment of the EMG wire or EEG headstage during the course of the experiment (1 old and 1 young animal were excluded).

For the highest order design, the four groups of mice were arranged in a 2 Age (Young * Old) x 2 (Control * SD) Between Factorial Design, to analyze the independent effect of Age group or Sleep condition, compared to the combined effect (or interaction) between the two manipulations. In all analyses, we first tested Age by Sleep interactions. If there was a significant interaction, we tested for simple effects of Age on each individual Sleep condition, and the simple Effects of Sleep condition on each individual Age group, all this through an analysis of contrasts. When there was no significant interaction, the main

effects analysis did not require post hoc tests since this was a 2x2 design. In some cases, the design required 1-way analysis (equivalent to t test since the variable had only two levels), while in other cases the design was more complex, requiring a 3-way type, e.g., 2x2 basic manipulation, as well as the temporal trial (moment) manipulation as a factor of repeated-measures.

Robust analyses of variance on trimmed means (Fw statistic) were conducted by using the method described by Wilcox (2012), based on the generalization of Algina and Olejnik (1984) from the Johansen (1980) matrix algebra of factorial designs. This statistic is distributed according to a Chi-square, whose degrees of freedom (df) correspond to the number of contrasts necessary to decompose the variability of the effect, as is the case in the numerator of parametric F ANOVA (e.g., df = 1 for main effects of Age, or Sleep Condition, and df = 1*1 or 1, for interaction of both). Robust contrasts were conducted by a t test trimmed variant (T_W on between, and Z_W on within factors), based on Yuen-Welch post hoc test with Rom's sequentially rejective method to control Type I error for multiple t tests [see details see, Wilcox, 2012]. Specifically, this robust t test is estimated from the squared standard error of trimmed means, calculated using the Winsorized variance. In the case of T_W, the degrees of freedom are estimated with a logic similar to that of the t-student for samples with variances uneven but replacing the standard error of the mean by the robust standard error of trimmed means. Specifically, the distribution of the test statistic is approximated using a Student T-distribution with degree of freedom determined by the error variability (i.e., sample variance) and sample sizes (Wilcox, 2012). In contrast, the Zw test does not have degrees of freedom associated with the test statistic since its value is based on a single pool of critical z values from a normal distribution, regardless of sample size. In order to gain sensitivity, given the complexity of some of the designs (e.g., 3-way mixed) and the presence of outliers, the probabilities associated with the Trimmed ANOVA were re-estimated using specific tests of first-order interactions (Patel and Hoel, 1973) and Bootstrap-t methods (Wilcox, 2012) in the case of second-order interactions. On the other hand, in the designs that included some variable of repeated-measures, the basic test of contrasts was re-estimated using Percentile Bootstrap (Wilcox, 2012). All the functions that allow the robust ANOVA to be carried out according to all the types of designs used in the research are specified below. Finally, in all these analytical steps, we added the estimated effect size from Wilcox robust "Explanatory Measures." Values of 0.15, 0.35, and 0.50 correspond to the three bands of interpretation of the effect size as small, moderate, and large, respectively, from Wilcox robust interpolation of classical 0.2, 0.5, and 0.8 Cohen bands. Statistical significance was set at alpha 0.05. Data are graphed using boxplots, plus the trimmed mean (trimmed = 0.2).

All statistical analyses were performed using GNU R software, version 4.0.0 (R Development Core Team, 2020) with *parallel, data.table*, *Hmisc*, and *ggplot2* libraries, as general libraries, and Wilcox' *Rallfun-v37.txt* library (https://dornsife.usc.edu/labs/rwilcox/software/) for specific robust ANOVAs. Ask for the functions *bbwtrim*, and *bbwtrimbt* for 3-way Mixed designs [e.g., 2 Age (Young, Old) x 2 Sleep (Control, SD) x 5xS Trials (HAB, T1, T2, T3, Test)]; *t2way, t2waybt, rimul, bdm2way, ESmainMCP,* and *esImcp* for 2-way Between designs [e.g., 2 Age (Young,Old) x 2 Sleep (Control, SD)]; *bwtrim, bwtrimbt, ESmainMCP*, and esImcp for 2-way Mixed designs [e.g., 2 (Young, Old) x 5xS Hours (Hour

1 to Hour 5)]; *t1way* for 1-way Between design [e.g., 2 Age (Young Control, Old Control)]; *yuen, yuenv2,* and *lincon* for contrasts (or t tests) with independent samples, and *yuendv2*, *rmmcp*, and *rmmismcp* for contrasts (or t tests) for dependent samples.

Supplementary Material

Refer to Web version on PubMed Central for supplementary material.

ACKNOWLEDGMENTS

This work has been funded by NSF (NSF/IOS 1924732 to I.A.M.) and NIH (R01 MH123260-01 to I.A.M.; RISE GMO60655 to M.R.L.;VA CDA IK2 BX004905 to D.S.U.; and F31 MH105161 and F32 HL143893 to R.K.Y.). We thank Sriharshini Muthukumar for running some behavioral experiments. In particular, we thank Fumi Katsumi, Robert E. Strecker, and James M. McNally, Department of Psychiatry, VA Boston Healthcare System and Harvard Medical School, for providing a validated automated spindle-detection code.

REFERENCES

Abel T, Havekes R, Saletin JM, and Walker MP (2013). Sleep, plasticity and memory from molecules to whole-brain networks. Curr. Biol 23, R774–R788. [PubMed: 24028961]

Algina J, and Olejnik SF (1984). Implementing the Welch-James procedure with factorial designs. Educ. Psychol. Meas 44, 39–48.

Altena E, Ramautar JR, Van Der Werf YD, and Van Someren EJ (2010). Do sleep complaints contribute to age-related cognitive decline? Prog. Brain Res 185, 181–205. [PubMed: 21075240]

Antony JW, Schönauer M, Staresina BP, and Cairney SA (2019). Sleep spindles and memory reprocessing. Trends Neurosci. 42, 1–3. [PubMed: 30340875]

Ásgeirsdóttir HN, Cohen SJ, and Stackman RW Jr. (2020). Object and place information processing by CA1 hippocampal neurons of C57BL/6J mice. J. Neurophysiol 123, 1247–1264. [PubMed: 32023149]

Bailey CH, Kandel ER, and Si K (2004). The persistence of long-term memory: a molecular approach to self-sustaining changes in learning-induced synaptic growth. Neuron 44, 49–57. [PubMed: 15450159]

Barnes CA, Suster MS, Shen J, and McNaughton BL (1997). Multistability of cognitive maps in the hippocampus of old rats. Nature 388, 272–275. [PubMed: 9230435]

Binder S, Baier PC, Mölle M, Inostroza M, Born J, and Marshall L (2012). Sleep enhances memory consolidation in the hippocampus-dependent object-place recognition task in rats. Neurobiol. Learn. Mem 97, 213–219. [PubMed: 22207008]

Buzsáki G (2015). Hippocampal sharp wave-ripple: a cognitive biomarker for episodic memory and planning. Hippocampus 25, 1073–1188. [PubMed: 26135716]

Castello-Domenech AB, Del Valle VI, Fernandez-Garrido J, Martinez-Martinez M, and Cauli O (2016). Sleep alterations in non-demented older individuals: the role of cortisol. Endocr. Metab. Immune Disord. Drug Targets 16, 174–180. [PubMed: 27908262]

Chatburn A, Coussens S, Lushington K, Kennedy D, Baumert M, and Kohler M (2013). Sleep spindle activity and cognitive performance in healthy children. Sleep (Basel) 36, 237–243.

Clawson BC, Durkin J, and Aton SJ (2016). Form and function of sleep spindles across the lifespan. Neural Plast. 2016, 6936381. [PubMed: 27190654]

Coenen AM, and van Luijtelaar EL (1985). Stress induced by three procedures of deprivation of paradoxical sleep. Physiol. Behav 35, 501–504. [PubMed: 4070421]

Cohen SJ, Munchow AH, Rios LM, Zhang G, Asgeirsdóttir HN, and Stackman RW Jr. (2013). The rodent hippocampus is essential for nonspatial object memory. Curr. Biol 23, 1685–1690. [PubMed: 23954431]

Contreras D, Destexhe A, Sejnowski TJ, and Steriade M (1996). Control of spatiotemporal coherence of a thalamic oscillation by corticothalamic feedback. Science 274, 771–774. [PubMed: 8864114]

Davis CJ, Clinton JM, Jewett KA, Zielinski MR, and Krueger JM (2011). Delta wave power: an independent sleep phenotype or epiphenomenon? J. Clin. Sleep Med 7 (5, Suppl), S16–S18. [PubMed: 22003323]

de Bruin EJ, van Run C, Staaks J, and Meijer AM (2017). Effects of sleep manipulation on cognitive functioning of adolescents: a systematic review. Sleep Med. Rev 32, 45–57. [PubMed: 27039223]

de Lavilléon G, Lacroix MM, Rondi-Reig L, and Benchenane K (2015). Explicit memory creation during sleep demonstrates a causal role of place cells in navigation. Nat. Neurosci 18, 493–495. [PubMed: 25751533]

Dispersyn G, Sauvet F, Gomez-Merino D, Ciret S, Drogou C, Leger D, Gallopin T, and Chennaoui M (2017). The homeostatic and circadian sleep recovery responses after total sleep deprivation in mice. J. Sleep Res 26, 531–538. [PubMed: 28425172]

Dix SL, and Aggleton JP (1999). Extending the spontaneous preference test of recognition: evidence of object-location and object-context recognition. Behav. Brain Res 99, 191–200. [PubMed: 10512585]

Drieu C, Todorova R, and Zugaro M (2018). Nested sequences of hippocampal assemblies during behavior support subsequent sleep replay. Science 362, 675–679. [PubMed: 30409880]

Espiritu JR (2008).Aging-related sleep changes. Clin. Geriatr. Med 24, 1–14, v. [PubMed: 18035227]

Gais S, and Born J (2004). Declarative memory consolidation: mechanisms acting during human sleep. Learn. Mem 11, 679–685. [PubMed: 15576885]

Gais S, Lucas B, and Born J (2006). Sleep after learning aids memory recall. Learn. Mem 13, 259–262. [PubMed: 16741280]

Geiger A, Huber R, Kurth S, Ringli M, Jenni OG, and Achermann P (2011). The sleep EEG as a marker of intellectual ability in school age children. Sleep (Basel) 34, 181–189.

Graves LA, Heller EA, Pack AI, and Abel T (2003). Sleep deprivation selectively impairs memory consolidation for contextual fear conditioning. Learn. Mem 10, 168–176. [PubMed: 12773581]

Grigg-Damberger MM (2012). The AASM Scoring Manual four years later. J. Clin. Sleep Med 8, 323–332. [PubMed: 22701392]

Halassa MM, Florian C, Fellin T, Munoz JR, Lee SY, Abel T, Haydon PG, and Frank MG (2009). Astrocytic modulation of sleep homeostasis and cognitive consequences of sleep loss. Neuron 61, 213–219. [PubMed: 19186164]

Harris KD, Hirase H, Leinekugel X, Henze DA, and Buzsáki G (2001). Temporal interaction between single spikes and complex spike bursts in hippocampal pyramidal cells. Neuron 32, 141–149. [PubMed: 11604145]

Hasan S, Dauvilliers Y, Mongrain V, Franken P, and Tafti M (2012). Age-related changes in sleep in inbred mice are genotype dependent. Neurobiol. Aging 33, 195.e13–195.e26.

Hasselmo ME (2006). The role of acetylcholine in learning and memory. Curr. Opin. Neurobiol 16, 710–715. [PubMed: 17011181]

Havekes R, Bruinenberg VM, Tudor JC, Ferri SL, Baumann A, Meerlo P, and Abel T (2014). Transiently increasing cAMP levels selectively in hippocampal excitatory neurons during sleep deprivation prevents memory deficits caused by sleep loss. J. Neurosci 34, 15715–15721. [PubMed: 25411499]

Huang YL, Liu RY, Wang QS, Van Someren EJ, Xu H, and Zhou JN (2002). Age-associated difference in circadian sleep-wake and rest-activity rhythms. Physiol. Behav 76, 597–603. [PubMed: 12126998]

Hutchison IC, and Rathore S (2015). The role of REM sleep theta activity in emotional memory. Front. Psychol 6, 1439. [PubMed: 26483709]

Hwaun E, and Colgin LL (2019). CA3 place cells that represent a novel waking experience are preferentially reactivated during sharp wave-ripples in subsequent sleep. Hippocampus 29, 921–938. [PubMed: 30891854]

Johansen S (1980). The Welch-James approximation to the distribution of the residual sum of squares in a weighted linear regression. Biometrika 67, 85–92.

Joo HR, and Frank LM (2018). The hippocampal sharp wave-ripple in memory retrieval for immediate use and consolidation. Nat. Rev. Neurosci 19, 744–757. [PubMed: 30356103]

Kaushal N, Nair D, Gozal D, and Ramesh V (2012). Socially isolated mice exhibit a blunted homeostatic sleep response to acute sleep deprivation compared to socially paired mice. Brain Res. 1454, 65–79. [PubMed: 22498175]

Keinath AT, Wang ME, Wann EG, Yuan RK, Dudman JT, and Muzzio IA (2014). Precise spatial coding is preserved along the longitudinal hippocampal axis. Hippocampus 24, 1533–1548. [PubMed: 25045084]

Kentros CG, Agnihotri NT, Streater S, Hawkins RD, and Kandel ER (2004). Increased attention to spatial context increases both place field stability and spatial memory. Neuron 42, 283–295. [PubMed: 15091343]

Krause AJ, Simon EB, Mander BA, Greer SM, Saletin JM, Goldstein-Piekarski AN, and Walker MP (2017). The sleep-deprived human brain. Nat. Rev. Neurosci 18, 404–18. [PubMed: 28515433]

Larkin MC, Lykken C, Tye LD, Wickelgren JG, and Frank LM (2014). Hippocampal output area CA1 broadcasts a generalized novelty signal during an object-place recognition task. Hippocampus 24, 773–783. [PubMed: 24596296]

Lee AK, and Wilson MA (2002). Memory of sequential experience in the hippocampus during slow wave sleep. Neuron 36, 1183–1194. [PubMed: 12495631]

Lester AW, Moffat SD, Wiener JM, Barnes CA, and Wolbers T (2017). The aging navigational system. Neuron 95, 1019–1035. [PubMed: 28858613]

Leutgeb S, Leutgeb JK, Barnes CA, Moser EI, McNaughton BL, and Moser MB (2005). Independent codes for spatial and episodic memory in hippocampal neuronal ensembles. Science 309, 619–623. [PubMed: 16040709]

Lister JP, and Barnes CA (2009). Neurobiological changes in the hippocampus during normative aging. Arch. Neurol 66, 829–833. [PubMed: 19597084]

Liu X, Ramirez S, Redondo RL, and Tonegawa S (2014). Identification and manipulation of memory engram cells. Cold Spring Harb. Symp. Quant. Biol 79, 59–65. [PubMed: 25637263]

Mendelson WB, and Bergmann BM (1999). EEG delta power during sleep in young and old rats. Neurobiol. Aging 20, 669–673. [PubMed: 10674433]

Miller DB, and O'Callaghan JP (2005). Aging, stress and the hippocampus. Ageing Res. Rev 4, 123–140. [PubMed: 15964248]

Mizumori SJ (2006). Hippocampal place fields: a neural code for episodic memory? Hippocampus 16, 685–690. [PubMed: 16881080]

Morgan E, Schumm LP, McClintock M, Waite L, and Lauderdale DS (2017). Sleep characteristics and daytime cortisol levels in older adults. Sleep (Basel) 40, zsx043.

Mumby DG, Gaskin S, Glenn MJ, Schramek TE, and Lehmann H (2002). Hippocampal damage and exploratory preferences in rats: memory for objects, places, and contexts. Learn. Mem 9, 49–57. [PubMed: 11992015]

Muzzio IA, Kentros C, and Kandel E (2009a).What is remembered? Role of attention on the encoding and retrieval of hippocampal representations. J. Physiol 587, 2837–2854. [PubMed: 19525568]

Muzzio IA, Levita L, Kulkarni J, Monaco J, Kentros C, Stead M, Abbott LF, and Kandel ER (2009b). Attention enhances the retrieval and stability of visuospatial and olfactory representations in the dorsal hippocampus. PLoS Biol. 7, e1000140. [PubMed: 19564903]

Naidoo N, Ferber M, Master M, Zhu Y, and Pack AI (2008). Aging impairs the unfolded protein response to sleep deprivation and leads to proapoptotic signaling. J. Neurosci 28, 6539–6548. [PubMed: 18579727]

Niethard N, Ngo HV, Ehrlich I, and Born J (2018). Cortical circuit activity underlying sleep slow oscillations and spindles. Proc. Natl. Acad. Sci. USA 115, E9220–E9229. [PubMed: 30209214]

O'Keefe J, and Dostrovsky J (1971). The hippocampus as a spatial map. Preliminary evidence from unit activity in the freely-moving rat. Brain Res. 34, 171–175. [PubMed: 5124915]

Ohayon MM, Carskadon MA, Guilleminault C, and Vitiello MV (2004). Meta-analysis of quantitative sleep parameters from childhood to old age in healthy individuals: developing normative sleep values across the human lifespan. Sleep 27, 1255–1273. [PubMed: 15586779]

Oliveira AM, Hawk JD, Abel T, and Havekes R (2010). Post-training reversible inactivation of the hippocampus enhances novel object recognition memory. Learn. Mem 17, 155–160. [PubMed: 20189960]

Pace-Schott EF, and Spencer RM (2015). Sleep-dependent memory consolidation in healthy aging and mild cognitive impairment. Curr. Top. Behav. Neurosci 25, 307–330. [PubMed: 24652608]

Palchykova S, Winsky-Sommerer R, Meerlo P, Dürr R, and Tobler I (2006). Sleep deprivation impairs object recognition in mice. Neurobiol. Learn. Mem 85, 263–271. [PubMed: 16423541]

Panagiotou M, Vyazovskiy VV, Meijer JH, and Deboer T (2017). Differences in electroencephalographic non-rapid-eye movement sleep slow-wave characteristics between young and old mice. Sci. Rep 7, 43656. [PubMed: 28255162]

Patel KM, and Hoel DG (1973). A nonparametric test for interaction in factorial experiments. J. Am. Stat. Assoc 68, 615–620.

Peyrache A, and Seibt J (2020). A mechanism for learning with sleep spindles. Philos. Trans. R. Soc. Lond. B Biol. Sci 375, 20190230. [PubMed: 32248788]

Poe GR (2017). Sleep is for forgetting. J. Neurosci 37, 464–473. [PubMed: 28100731]

Powers MM, and Clark G (1955). An evaluation of cresyl echt violet acetate as a Nissl stain. Stain Technol. 30, 83–88. [PubMed: 14358982]

Preston AR, and Eichenbaum H (2013). Interplay of hippocampus and prefrontal cortex in memory. Curr. Biol 23, R764–R773. [PubMed: 24028960]

Prince TM, Wimmer M, Choi J, Havekes R, Aton S, and Abel T (2014). Sleep deprivation during a specific 3-hour time window post-training impairs hippocampal synaptic plasticity and memory. Neurobiol. Learn. Mem 109, 122–130. [PubMed: 24380868]

R Development Core Team (2020). R: A language and environment for statistical computing (R Foundation for Statistical Computing).

Ranck JB Jr. (1973). Studies on single neurons in dorsal hippocampal formation and septum in unrestrained rats. I. Behavioral correlates and firing repertoires. Exp. Neurol 41, 461–531. [PubMed: 4355646]

Rasch B, and Born J (2013). About sleep's role in memory. Physiol. Rev 93, 681–766. [PubMed: 23589831]

Rosenzweig ES, and Barnes CA (2003). Impact of aging on hippocampal function: plasticity, network dynamics, and cognition. Prog. Neurobiol 69, 143–179. [PubMed: 12758108]

Rosinvil T, Lafortune M, Sekerovic Z, Bouchard M, Dubé J, Latulipe-Loiselle A, Martin N, Lina JM, and Carrier J (2015). Age-related changes in sleep spindles characteristics during daytime recovery following a 25-hour sleep deprivation. Front. Hum. Neurosci 9, 323. [PubMed: 26089788]

Rowland DC, Yanovich Y, and Kentros CG (2011). A stable hippocampal representation of a space requires its direct experience. Proc. Natl. Acad. Sci. USA 108, 14654–14658. [PubMed: 21852575]

Rytkönen KM, Zitting J, and Porkka-Heiskanen T (2011). Automated sleep scoring in rats and mice using the naive Bayes classifier. J. Neurosci. Methods 202, 60–64. [PubMed: 21884727]

Saletin JM, Goldstein-Piekarski AN, Greer SM, Stark S, Stark CE, and Walker MP (2016). Human hippocampal structure: a novel biomarker predicting mnemonic vulnerability to, and recovery from, sleep deprivation. J. Neurosci 36, 2355–2363. [PubMed: 26911684]

Sawangjit A, Oyanedel CN, Niethard N, Salazar C, Born J, and Inostroza M (2018). The hippocampus is crucial for forming non-hippocampal long-term memory during sleep. Nature 564, 109–113. [PubMed: 30429612]

Schimanski LA, and Barnes CA (2010). Neural protein synthesis during aging: effects on plasticity and memory. Front. Aging Neurosci 2, 26. [PubMed: 20802800]

Schmitzer-Torbert N, Jackson J, Henze D, Harris K, and Redish AD (2005). Quantitative measures of cluster quality for use in extracellular recordings. Neuroscience 131, 1–11. [PubMed: 15680687]

Schoenenberger P, O'Neill J, and Csicsvari J (2016). Activity-dependent plasticity of hippocampal place maps. Nat. Commun 7, 11824. [PubMed: 27282121]

Seibt J, Richard CJ, Sigl-Glöckner J, Takahashi N, Kaplan DI, Doron G, de Limoges D, Bocklisch C, and Larkum ME (2017). Cortical dendritic activity correlates with spindle-rich oscillations during sleep in rodents. Nat. Commun 8, 684. [PubMed: 28947770]

Skaggs W, McNaughton B, Gothard K, and Markus E (1993). An information-theoretic approach to deciphering the hippocampal code. In Advances in Neural Information Processing, Hanson S, Cowan J, and Giles C, eds. (Morgan Kaufmann), pp. 1030–1037.

Smith C (2001). Sleep states and memory processes in humans: procedural versus declarative memory systems. Sleep Med. Rev 5, 491–506. [PubMed: 12531156]

Smith DM, and Mizumori SJ (2006). Hippocampal place cells, context, and episodic memory. Hippocampus 16, 716–729. [PubMed: 16897724]

Smith C, and Rose GM (1996). Evidence for a paradoxical sleep window for place learning in the Morris water maze. Physiol. Behav 59, 93–97. [PubMed: 8848497]

Sportiche N, Suntsova N, Methippara M, Bashir T, Mitrani B, Szymusiak R, and McGinty D (2010). Sustained sleep fragmentation results in delayed changes in hippocampal-dependent cognitive function associated with reduced dentate gyrus neurogenesis. Neuroscience 170, 247–258. [PubMed: 20600652]

Squire LR, and Zola SM (1998). Episodic memory, semantic memory, and amnesia. Hippocampus 8, 205–211. [PubMed: 9662135]

Squire LR, Genzel L, Wixted JT, and Morris RG (2015). Memory consolidation. Cold Spring Harb. Perspect. Biol 7, a021766. [PubMed: 26238360]

Stickgold R, and Walker MP (2013). Sleep-dependent memory triage: evolving generalization through selective processing. Nat. Neurosci 16, 139–145. [PubMed: 23354387]

Taillard J, Sagaspe P, Berthomier C, Brandewinder M, Amieva H, Dartigues JF, Rainfray M, Harston S, Micoulaud-Franchi JA, and Philip P (2019). Non-REM sleep characteristics predict early cognitive impairment in an aging population. Front. Neurol 10, 197. [PubMed: 30918496]

Tanaka KZ, He H, Tomar A, Niisato K, Huang AJY, and McHugh TJ (2018). The hippocampal engram maps experience but not place. Science 361, 392–397. [PubMed: 30049878]

Tartar JL, Ward CP, McKenna JT, Thakkar M, Arrigoni E, McCarley RW, Brown RE, and Strecker RE (2006). Hippocampal synaptic plasticity and spatial learning are impaired in a rat model of sleep fragmentation. Eur. J. Neurosci 23, 2739–2748. [PubMed: 16817877]

Tobler I, Murison R, Ursin R, Ursin H, and Borbély AA (1983). The effect of sleep deprivation and recovery sleep on plasma corticosterone in the rat. Neurosci. Lett 35, 297–300. [PubMed: 6843904]

Tononi G, and Cirelli C (2006). Sleep function and synaptic homeostasis. Sleep Med. Rev 10, 49–62. [PubMed: 16376591]

Tononi G, and Cirelli C (2014). Sleep and the price of plasticity: from synaptic and cellular homeostasis to memory consolidation and integration. Neuron 81, 12–34. [PubMed: 24411729]

Ulrich D (2016). Sleep spindles as facilitators of memory formation and learning. Neural Plast. 2016, 1796715. [PubMed: 27119026]

Uygun DS, Katsuki F, Bolortuya Y, Aguilar DD, McKenna JT, Thankachan S, McCarley RW, Basheer R, Brown RE, Strecker RE, and McNally JM (2019). Validation of an automated sleep spindle detection method for mouse electroencephalography. Sleep (Basel) 42, zsy218.

Varela C, and Wilson MA (2020). mPFC spindle cycles organize sparse thalamic activation and recently active CA1 cells during non-REM sleep. eLife 9, e48881. [PubMed: 32525480]

Wang ME, Wann EG, Yuan RK, Ramos Álvarez MM, Stead SM, and Muzzio IA (2012). Long-term stabilization of place cell remapping produced by a fearful experience. J. Neurosci 32, 15802–15814. [PubMed: 23136419]

Wang ME, Yuan RK, Keinath AT, Ramos Álvarez MM, and Muzzio IA (2015). Extinction of learned fear induces hippocampal place cell remapping. J. Neurosci 35, 9122–9136. [PubMed: 26085635]

Ward CP, McCarley RW, and Strecker RE (2009a). Experimental sleep fragmentation impairs spatial reference but not working memory in Fischer/Brown Norway rats. J. Sleep Res 18, 238–244. [PubMed: 19645967]

Ward CP, McCoy JG, McKenna JT, Connolly NP, McCarley RW, and Strecker RE (2009b). Spatial learning and memory deficits following exposure to 24 h of sleep fragmentation or intermittent hypoxia in a rat model of obstructive sleep apnea. Brain Res. 1294, 128–137. [PubMed: 19643093]

Wennberg AM, Canham SL, Smith MT, and Spira AP (2013). Optimizing sleep in older adults: treating insomnia. Maturitas 76, 247–252. [PubMed: 23746664]

Wilcox RR (2012). Introduction to Robust Estimation Hypothesis Testing(Academic).

Wilson M, Permito R, English A, Albritton S, Coogle C, and Van Dongen HPA (2019). Performanceand sleepiness in nursesworking 12-h day shiftsor night shifts in a community hospital. Accid. Anal. Prev 126, 43–46. [PubMed: 28987265]

Wimmer ME, Hernandez PJ, Blackwell J, and Abel T (2012). Aging impairs hippocampus-dependent long-term memory for object location in mice. Neurobiol. Aging 33, 2220–2224. [PubMed: 21872364]

Wimmer ME, Rising J, Galante RJ, Wyner A, Pack AI, and Abel T (2013). Aging in mice reduces the ability to sustain sleep/wake states. PLoS ONE 8, e81880. [PubMed: 24358130]

Winsky-Sommerer R, Knapman A, Fedele DE, Schofield CM, Vyazovskiy VV, Rudolph U, Huguenard JR, Fritschy JM, and Tobler I (2008). Normal sleep homeostasis and lack of epilepsy phenotype in GABA A receptor alpha3 subunit-knockout mice. Neuroscience 154, 595–605. [PubMed: 18485607]

Highlights

- Sleep deprivation improves memory in old mice but worsens it in young ones
- Sleep deprivation decreases hippocampal flexibility and spindle counts in young mice
- Increased spindle counts are associated with improved memory in old mice
- Sleep deprivation improves the quality of hippocampal representations in old mice

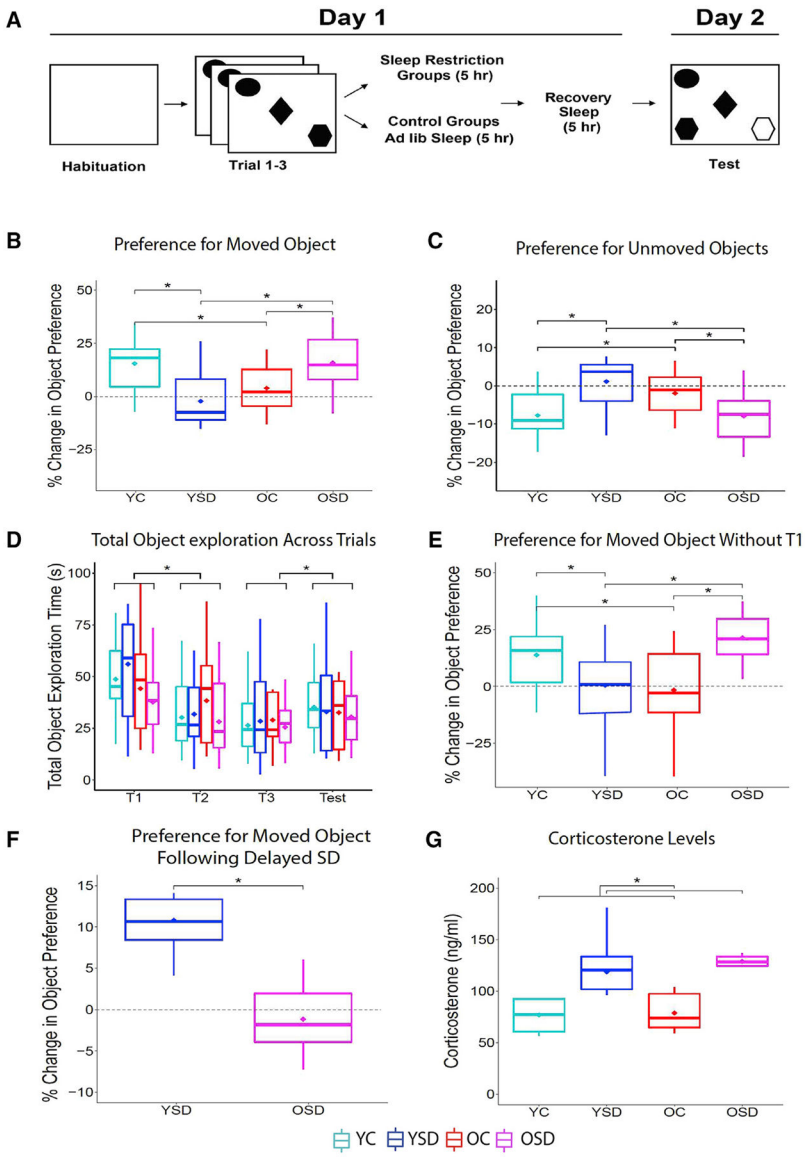

Figure 1. OPR behavioral performance

(A) Schematic of behavioral paradigm.

(B) Percent change in preference for displaced object (young control [YC]: n = 16; young SD [YSD]: n = 15; old control [OC]: n = 13; old SD [OSD]: n = 15).

(C) Total object exploration time during training and testing.

(D) Percent change in preference for displaced object in young (n = 6) and old (n = 7) mice receiving delayed SD (5 h after training).

(E) Levels of plasma corticosterone (YC: n = 5; OC: n = 5; YSD: n = 5; OSD: n = 6).

In all figures, data are graphed using boxplots where the inner line corresponds to the median, the lower box the first quartile, the upper box the third quartile, the extending lines (whiskers) the minimum and maximum, and the diamond the trimmed mean used for analysis. The trimmed mean was set at 0.2 for all age groups and sleep conditions. T1–T3,

training trials. Asterisks (*) represent significance using alpha = 0.05. Statistical details are in Data S1.

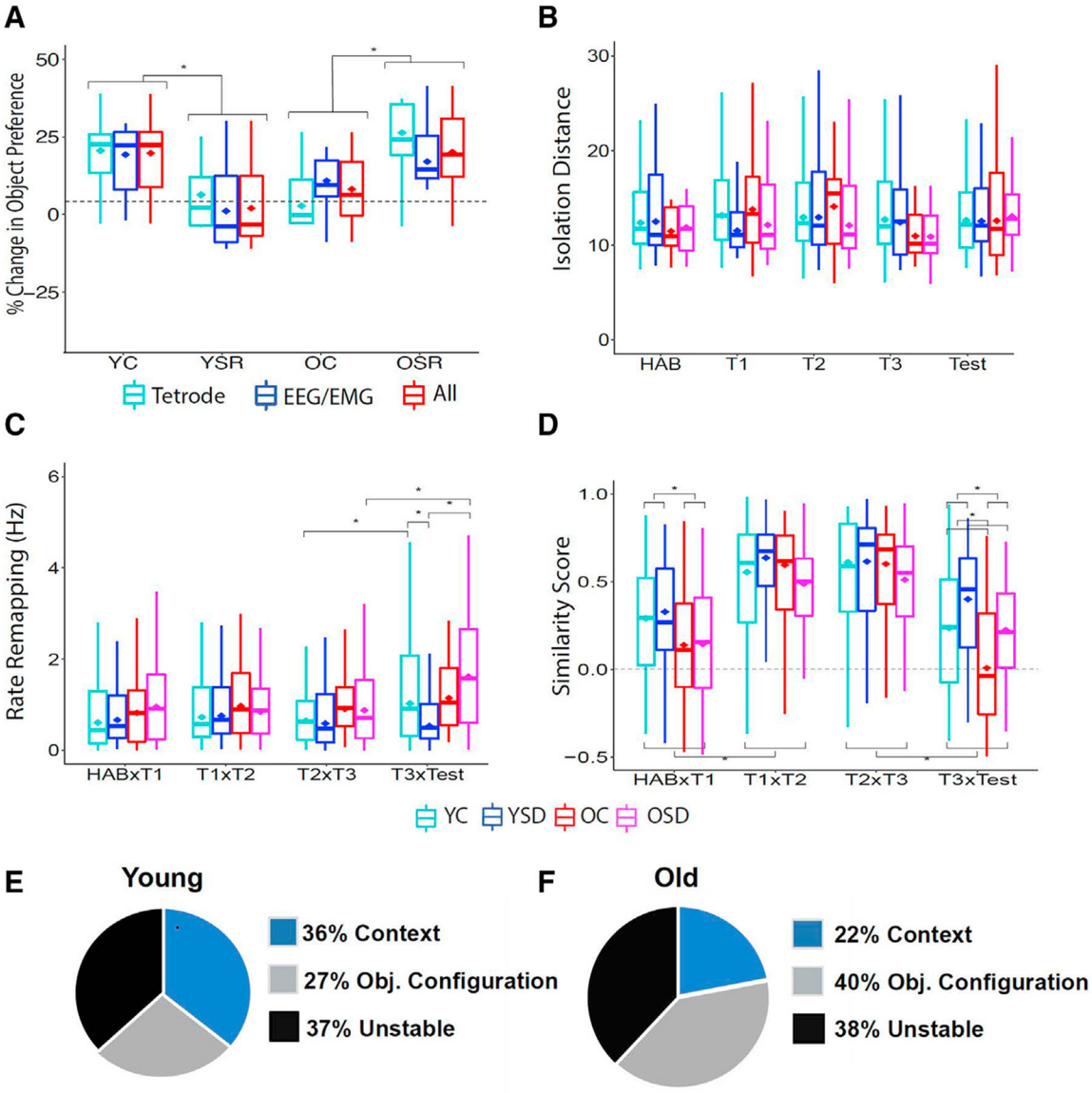

Figure 2. Rate and global remapping and percentage of different cell types during OPR performance

(A) Performance comparing animals implanted with tetrodes or EEG/EMG.

(B) Cluster isolation distance.

(C) Average rate remapping for all groups across trials.

(D) Average global remapping (map similarity) for all groups across trials.

(E and F) Percentage of context, object configuration, and unstable cells recorded in young (E) and old (F) mice.

YC: 6 mice, 60 cells, range of cells per animal: 6–16; YSD: 4 mice, 50 cells, range of cells per animal: 8–18; OC: 5 mice, 36 cells, range of cells per animal: 5–13; OSD: 5 mice, 41 cells: range of cells per animal: 4–13. Hab, habituation. Asterisks (*) represent significance using alpha = 0.05. Statistical details are in Data S1.

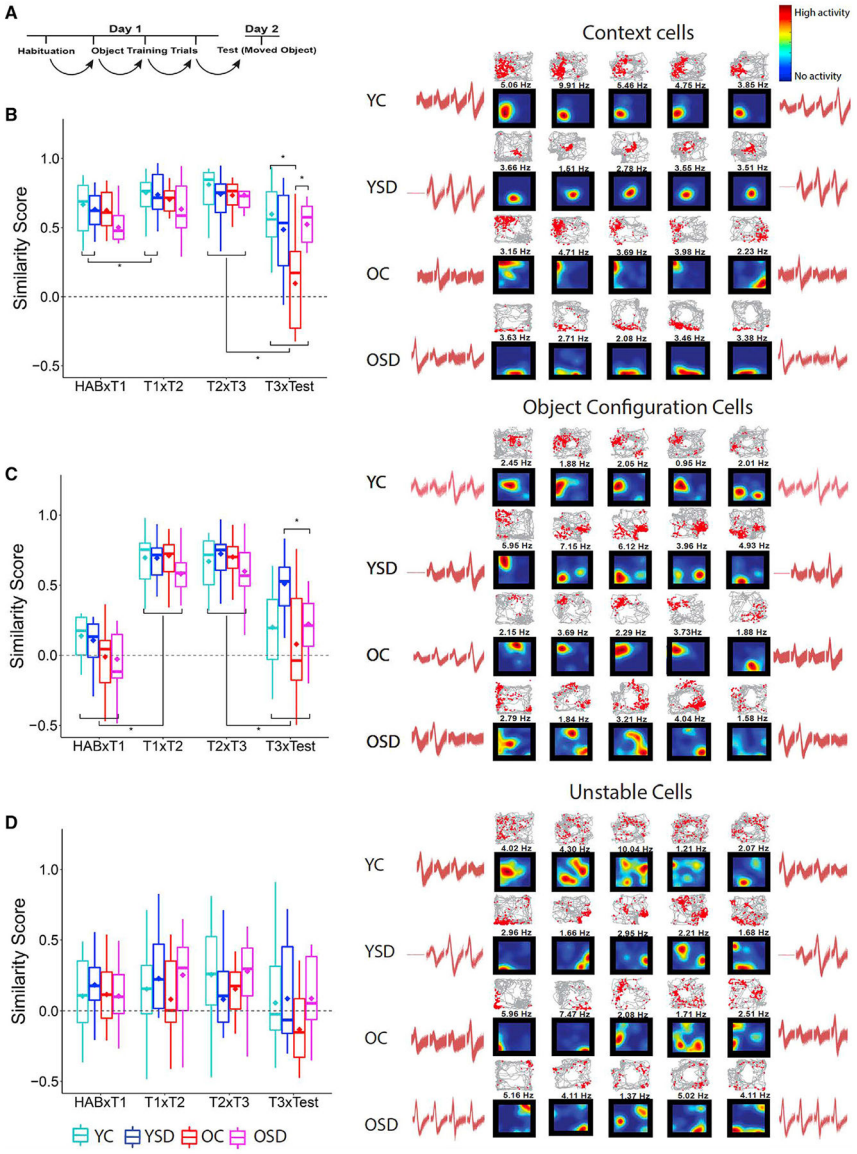

Figure 3. Cell type remapping across sessions during OPR performance

(A) Schematic of correlation design.

(B–D) Average global remapping of context (B), object configuration (C), and unstable (D) cells across trials and corresponding examples of color-coded place cell rate maps, trajectory spike maps, and waveforms. In all place cell maps, blue indicates that the animal has visited a region, but the cell has not fired; vivid colors indicate high neuronal activity (as shown in the color bar at the upper right corner).The number on top of each map indicates the peak firing rate (Hz) used to normalize the map colors. In all trajectory maps, red dots represent location of action potentials and gray lines the path of the animal. Waveform similarity indicates recording stability during the 24-h period of training and testing.

Context cells: YC = 23 cells; YSD = 20 cells; OC = 8 cells; OSD = 9 cells. Object cells: YC: 15 cells; YSD: 13 cells; OC: 17 cells; OSD: 14 cells. Unstable cells: YC = 22 cells; YSD =

17 cells; OC = 11 cells; OSD = 18 cells. Asterisks (*) represent significance using alpha = 0.05. Statistical details are in Data S1.

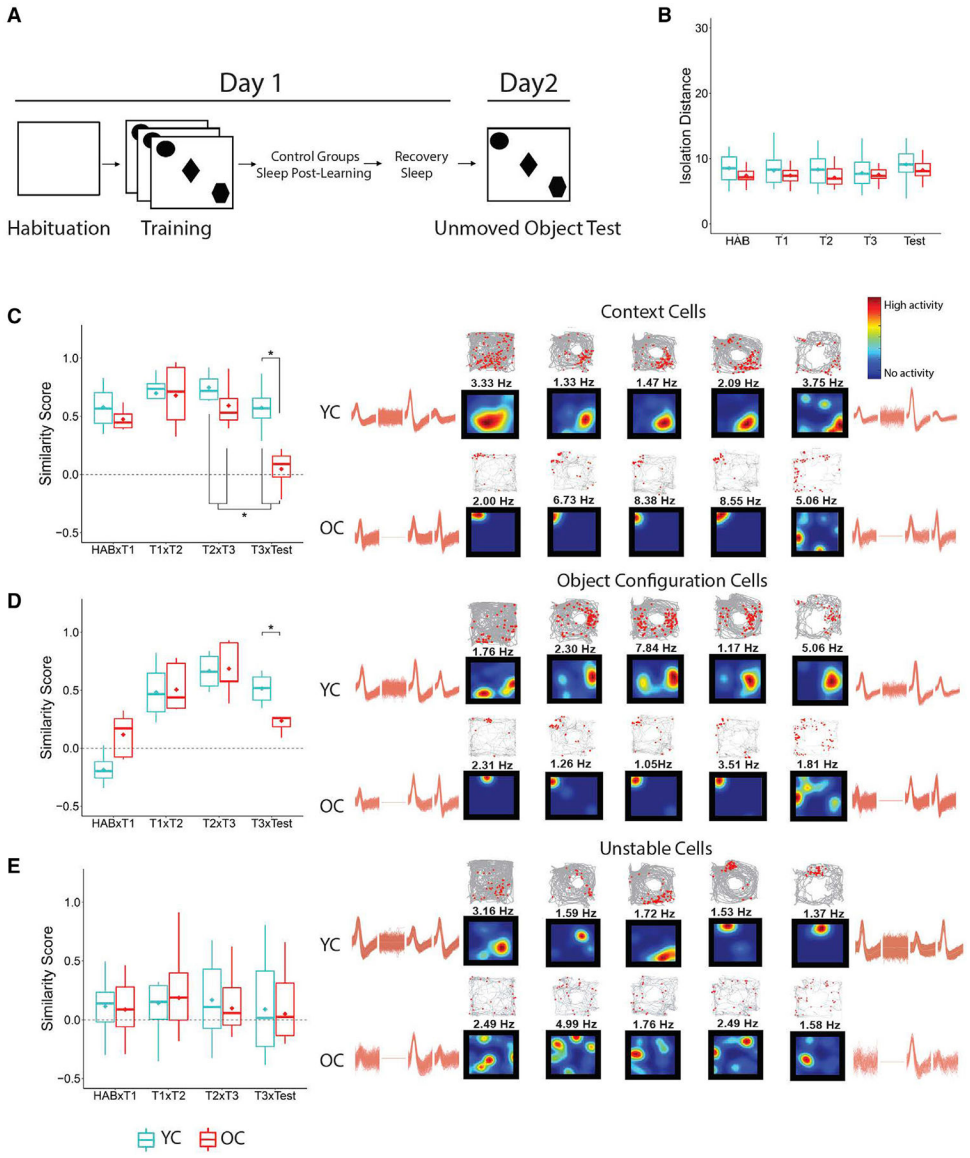

Figure 4. Place cell stability during unmoved object control task

(A) Schematics of the task.

(B) Isolation distance.

(C–E) Examples of context (C), object configuration (D), and unstable (E) rate maps, trajectory spike maps, and waveforms recorded from young and old control mice trained in the unmoved object control task. Color code is the same as Figure 3. Waveform similarity indicates recording stability during the 24-h period of training and testing.

YC: 3 mice, 30 cells; OC: 4 mice, 24 cells. Asterisks (*) represent significance using alpha = 0.05. Statistical details are in Data S1.

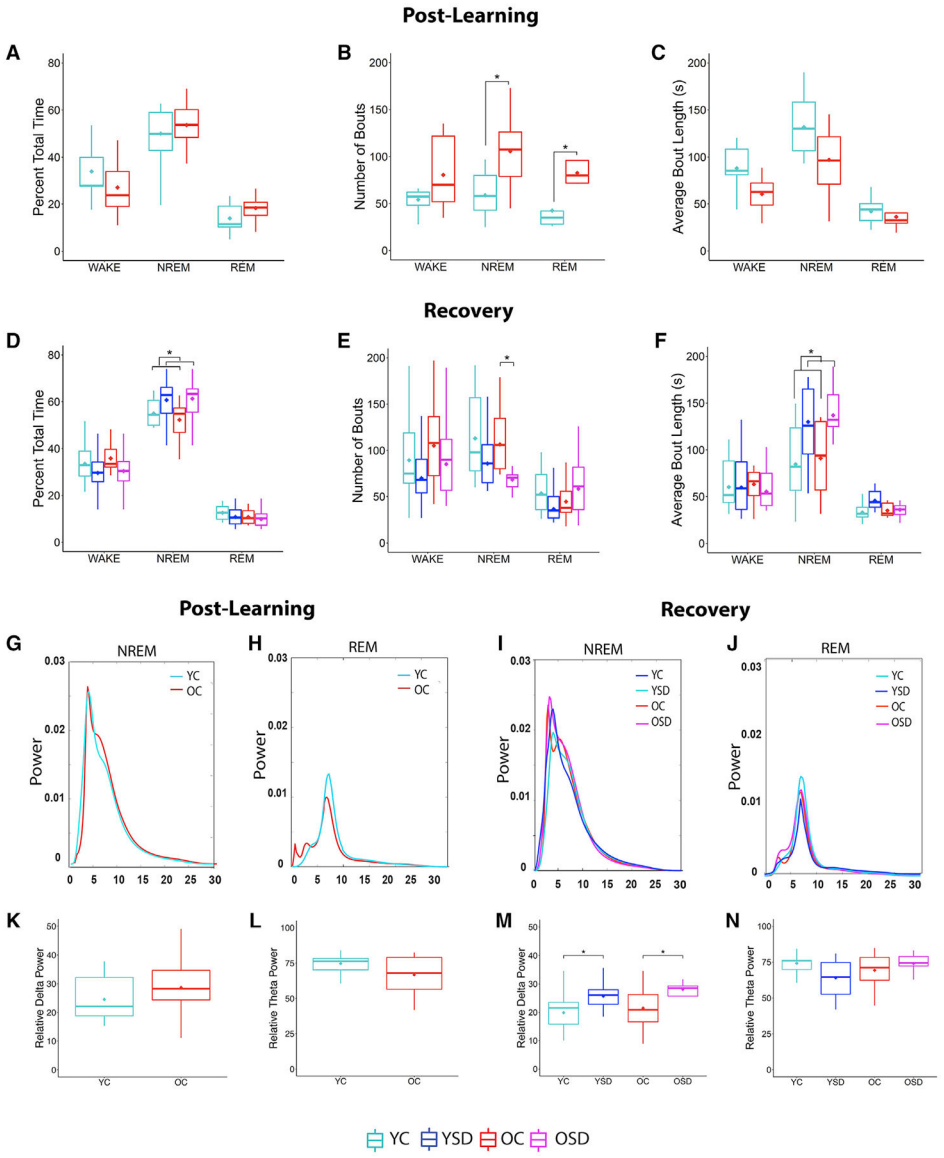

Figure 5. Sleep patterns, average power spectra, and relative delta (RDP) and theta (RTP) during post-training and recovery sleep in young and old mice

(A–C) Percentage of total time (A), number of bouts (B), and bout length (C) in wake, NREM, and REM during post-training sleep in young and old control mice.

(D–F) Percentage of total time (D), number of bouts (E), and bout length (F) in wake, NREM, and REM during recovery sleep in control and SD groups.

(G–J) Average NREM/REM power spectra during post-learning (G and H) and recovery (I and J).

(K–N) Average NREM/REM RDP and RTP during post-learning (K and L) and recovery (M and N).

RDP: 0.25–4 Hz; RTP: 4–10 Hz. YC: n = 11; YSD: n = 11; old control (n = 8); old SD (n = 10). Asterisks (*) represent significance using alpha = 0.05. Statistical details are in Data S1.

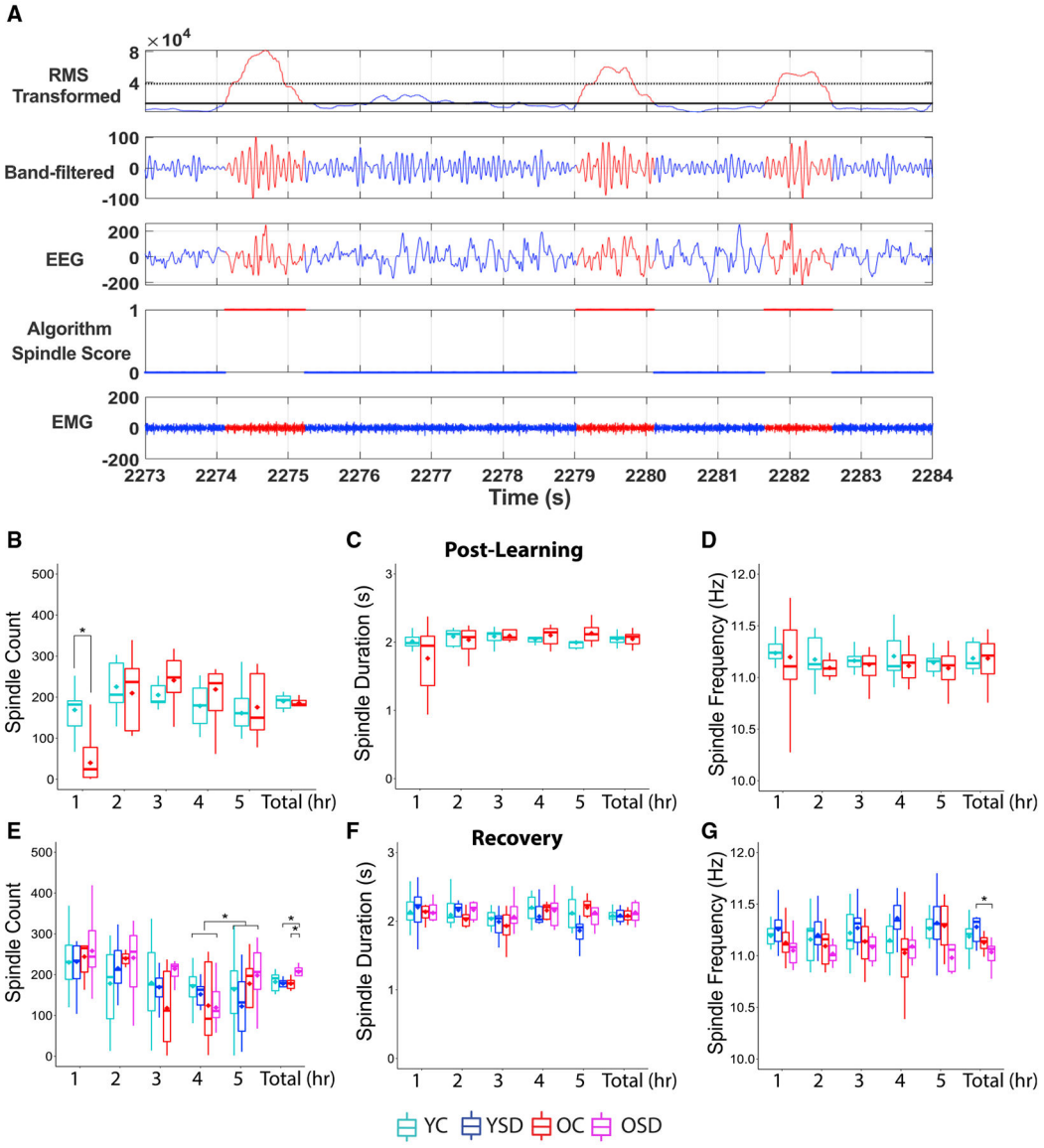

Figure 6. Spindle characteristics

(A) Representation of the automated spindle-detection method. Top panel shows cubed root-mean-square (RMS) of the filtered EEG. The second, third, and fourth panels show the band-pass filtered EEG, the unfiltered EEG, and the results of the spindle detection, respectively. The bottom panel depicts the corresponding EMG signal. Red marks the regions of the signal where spindles are detected; 1 indicates the presence and 0 the absence of spindles.

(B–D) Spindle counts (B), duration (C), and frequency (D) during the post-learning sleep.

(E–G) Spindle numbers (E), duration (F), and frequency (G) during recovery.

YC: n = 11; YSD: n = 11; OC: n = 8; OSD: n = 10. Asterisks (*) represent significance using alpha = 0.05. Statistical details are in Data S1.

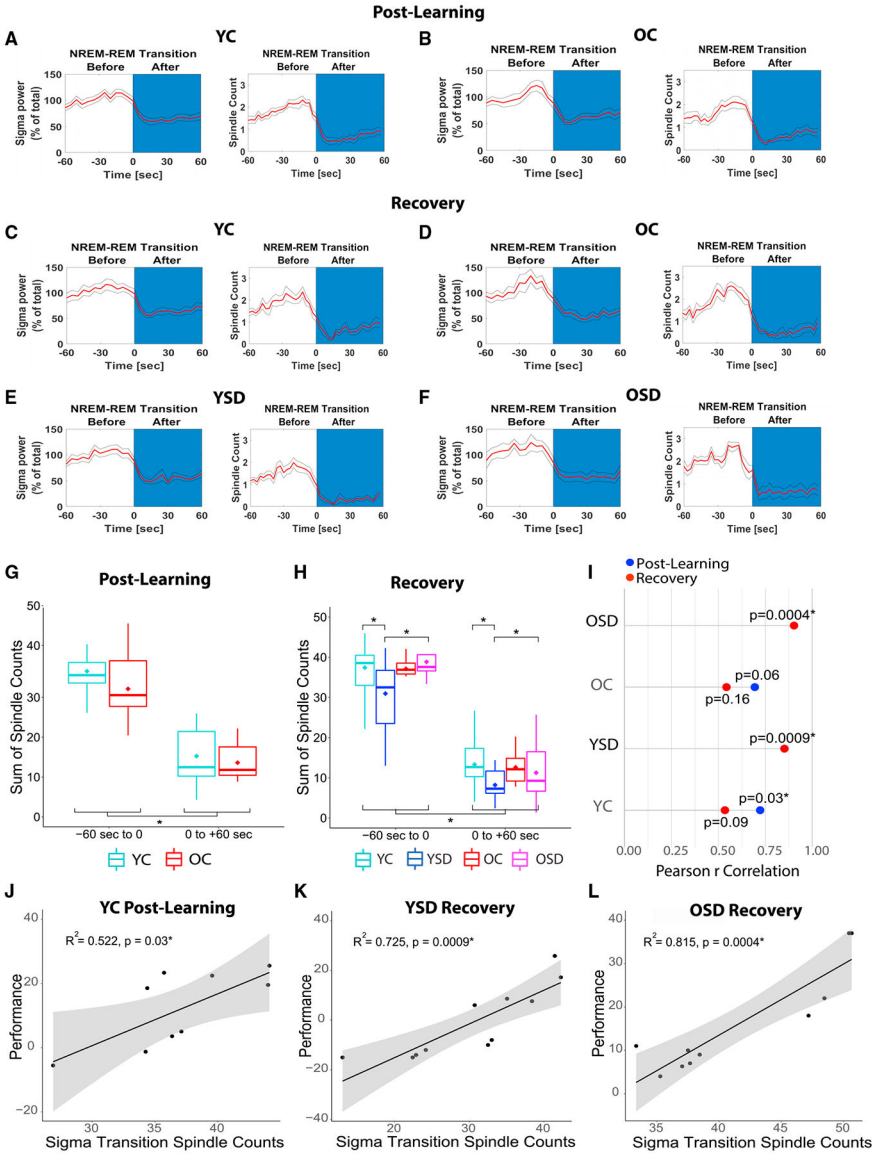

Figure 7. Spindle counts during NREM/REM sigma transitions and memory performance

(A–F) Plots showing NREM/REM sigma transitions for controls during post-learning (A and B) and control and SD groups during recovery (C–F).

(G and H) Spindle counts during post-learning (G) and recovery (H) NREM/REM sigma transitions.

(I) Correlations between OPR memory performance and spindle counts during NREM/REM sigma transitions.

(J–L) Scatted plots showing significant correlations between performance and spindle counts during sigma transitions in YC post-learning (J), and YSD (K) and OSD (L) during recovery.

YC: n = 11; YSD: n = 11; OC: n = 8; OSD: n = 10. Asterisks (*) represent significance using alpha = 0.05. Statistical details are in Data S1.

KEY RESOURCES TABLE

REAGENT or RESOURCE	SOURCE	IDENTIFIER
Deposited data		
Raw data	This paper	https://data.mendeley.com/datasets/yy3kbv3v8n/1
Experimental models: organisms/strains		
C57BL/6J	The Jackson Laboratory	000664 Aged 000664
Software and algorithms		
MATLAB custom code for place cells analysis	This paper	https://github.com/marcnormandin/muzziolab_sleep_tetrodes_objecttask
Custom GNU R code	This paper (R Development Core Team, 2020)	https://github.com/ManuMi68/MuLaNA
EEG custom code	This paper	https://github.com/marcnormandin/muzziolab_eeg_2021
Cluster cutting program	MClust	http://redishlab.neuroscience.umn.edu/mclust/MClust.html